Published in final edited form as:
SIAM J Appl Dyn Syst. ; 12(3): 1474–1514. doi:10.1137/120900435.

Locally Contractive Dynamics in Generalized Integrate-and-Fire Neurons*

Nicolas D. Jimenez[†], **Stefan Mihalas**[†], **Richard Brown**[‡], **Ernst Niebur**[§], and **Jonathan Rubin**[¶]

Nicolas D. Jimenez: njimene2@stanford.edu; Stefan Mihalas: stefanm@alleninstitute.org; Richard Brown: brown@math.jhu.edu; Ernst Niebur: niebur@jhu.edu; Jonathan Rubin: jonrubin@pitt.edu

[†]Allen Institute for Brain Science, Seattle, WA 98103

[‡]Department of Mathematics, Johns Hopkins University, Baltimore, MD 21218

[§]Department of Neuroscience, Johns Hopkins University, Baltimore, MD 21205

[¶]Department of Mathematics, University of Pittsburgh, Pittsburgh, PA 15260

Abstract

Integrate-and-fire models of biological neurons combine differential equations with discrete spike events. In the simplest case, the reset of the neuronal voltage to its resting value is the only spike event. The response of such a model to constant input injection is limited to tonic spiking. We here study a generalized model in which two simple spike-induced currents are added. We show that this neuron exhibits not only tonic spiking at various frequencies but also the commonly observed neuronal bursting. Using analytical and numerical approaches, we show that this model can be reduced to a one-dimensional map of the adaptation variable and that this map is locally contractive over a broad set of parameter values. We derive a sufficient analytical condition on the parameters for the map to be globally contractive, in which case all orbits tend to a tonic spiking state determined by the fixed point of the return map. We then show that bursting is caused by a discontinuity in the return map, in which case the map is *piecewise contractive*. We perform a detailed analysis of a class of piecewise contractive maps that we call bursting maps and show that they robustly generate stable bursting behavior. To the best of our knowledge, this work is the first to point out the intimate connection between bursting dynamics and piecewise contractive maps. Finally, we discuss bifurcations in this return map, which cause transitions between spiking patterns.

Keywords

integrate-and-fire; hybrid dynamical systems; Mihalas–Niebur neuron; bursting; contraction analysis; piecewise contractions

1. Introduction

A pervasive issue in computational neuroscience is the tradeoff between a neural model's accuracy and the computational cost of its implementation. Models that include details of biophysical ion channels, such as the Hodgkin–Huxley model, are considered very accurate, especially if they also take into account the detailed morphology of the cell. Unfortunately, such models are computationally very expensive and their specification requires many

*This work was supported by Office of Naval Research MURI grant N000141010278, National Institutes of Health/NEI grant R01EY016281, NSF award DMS 1021701, and a Johns Hopkins DURA research grant.

parameters. On the other hand, integrate-and-fire models without spatial extension are capable of reproducing basic neuronal behaviors while being far less computationally expensive and requiring far fewer parameters. Thus, parameter estimation from biological data is more tractable for these simplified neural models, and these lower-dimensional models allow for a systematic exploration of parameter space.

The leaky integrate-and-fire neuron appeared in the 1960s (see Brunel and van Rossum, 2007 for a review). All integrate-and-fire models use a differential equation to describe the transmembrane voltage of a neuron between action potentials ("spikes"). Given that spikes are highly stereotyped, the models omit detailed simulations of action potentials and replace them with simple instantaneous events. The sequence of times of these spiking events constitutes the output of the neuron. In addition, during a spiking event the transmembrane voltage is modified. In the simplest case (Knight, 1972), this modification is a reset of the voltage to its resting value, usually chosen as zero. In response to constant input, after a transient, the model's response is limited to generating sequences of action potentials with constant frequency ("tonic spiking"). Obviously, this frequency vanishes for sufficiently small input currents.

Despite its simplicity, the leaky integrate-and-fire neuron continues to be used in a large number of applications. Nevertheless, it is well known that the repertoire of biological neurons is not limited to tonic firing. To capture these richer behaviors, a number of generalized integrate-and-fire models have been proposed (for a review see Izhikevich, 2004). In this study, we consider a particular generalized integrate-and-fire model and focus primarily on how it can represent the two most commonly observed firing patterns (other than adaptation, which can be seen as a transient). One is tonic firing, already described, and the other is bursting, which is the generation of a sequence of action potentials in rapid progression followed by a silent period after which the process recommences. While there are other methods for adding bursting to a neuron model's repertoire, we will show that a very simple generalization of the leaky integrate-and-fire neuron, the addition of spike-induced currents, suffices.

The rigorous study of spiking neuron models is an active area in applied mathematics. Spiking models involving resets are examples of hybrid systems. Hybrid systems are generally defined as dynamical systems that exhibit both continuous and discrete dynamical behavior. This class of dynamical systems, however, is vast and admits many subclasses (see Henzinger, 1996 for a review). The best understood class of hybrid systems is that known as variable structure systems. These systems are of the following form:

$$\dot{\mathbf{x}}=\varphi(\mathbf{x},t), \quad (1.1)$$

where the state vector $\mathbf{x} \in \mathbb{R}^n$ is continuous and the function $\phi(\mathbf{x}, t) : \mathbb{R}^n \times \mathbb{R} \to \mathbb{R}^n$ is piecewise continuous with finitely many continuous pieces. When the state trajectory $\mathbf{x}$ crosses certain boundaries in the phase space, the function $\phi(\mathbf{x}, t)$ experiences a discontinuity.

On the other hand, in spiking neural models, the state trajectory is discontinuous, while the dynamical function $\phi(\mathbf{x}, t)$ remains constant. These systems are sometimes called impulsive dynamical systems (Haddad, Chellaboina, and Kablar, 2001), and their analysis requires tools different from those employed in the study of the more common switching-type hybrid systems frequently considered in the engineering and control literature. Later in this work, we point out an interesting connection between these two classes of hybrid systems: both naturally admit symbolic representations based on phase-space partitions.

In this paper, we take a similar approach to that of Touboul and Brette (2009) and provide a thorough analysis of the dynamics of a particular hybrid spiking model. The study of Touboul and Brette (2009), like ours, analyzes spiking patterns through an appropriately defined one-dimensional discrete map. This discrete map is defined based on reset to a line of possible values and maps a reset value after a spike to the reset value after the next spike. The analysis of the orbits generated by a map of this form in Touboul and Brette (2009), however, is complicated by the fact that the continuous dynamics are nonlinear. This nonlinearity necessarily complicates the relationship between the properties of the continuous system and those of the discrete map. In contrast, we shall see in section 3 that a linear model is sufficient for generating tonic spiking and bursting, and this formulation greatly facilitates the analysis of model solutions.

The maps considered by Touboul and Brette (2009) and Izhikevich and Hoppensteadt (2004) generate bursting patterns through limit cycles (a review of map-based approaches to neuronal dynamics can be found in Ibarz, Casado, and Sanjuán (2011); see also section 7). In both cases, the maps are continuous. Touboul and Brette (2009) make the following important observation: if there is a periodic bursting orbit of period 3, then there must exist periodic orbits of all periods. This follows directly from a theorem proved by Sharkovskiĭ (1995). This property is unfortunate from the point of view of neural coding, since it indicates that it is problematic to model intrinsic bursting of period 3 with a one-dimensional continuous map, as one must ensure that the orbits of other periods are unstable. It seems unlikely that real neurons are affected in an appreciable way by this mathematical difficulty.

The immediate consequence of this result is that, to the extent that intrinsic bursting of period 3 can be modeled by a class of one-dimensional maps, these maps cannot be continuous. In fact, discontinuous map models of neurons have previously been explored by Nagumo and Sato (1972), Rulkov (2002), Shilnikov and Rulkov (2003), Medvedev (2005), Manica, Medvedev, and Rubin (2010), and Lajoie and Shea-Brown (2011). Nagumo and Sato consider a piecewise linear map and give a condition for an individual orbit to be periodic. However, for general models with linear state dynamics between spikes, the adaptation map is nonlinear due to the nontrivial dependence of the post-spike assignment on initial conditions. Thus, Sato and Nagumo's work is particular to their map definition. In this work, we shall generalize their findings to a larger class of dynamical systems: those with piecewise contractive one-dimensional representations.

Although earlier work on map models of neurons does not fit into the piecewise contraction framework, piecewise contractive maps have been studied in the mathematical literature as a natural extension to the study of piecewise isometries and interval exchange transformations (see Bruin and Deane, 2009; Brémont, 2006; Gambaudo and Tresser, 1988; Catsigeras and Budelli, 2011). Piecewise contractive maps $\Phi : V \to V$, where V is a metric space, satisfy the contractive property $d(x, y) > d(\Phi(x), \Phi(y))$ but only when there is an i such that $x, y \in S_i$, where $\{S_i\}_{i=1}^{n}$ is a partitioning of the domain of Φ such that $V = \cup S_i$ and $S_i \cap S_j = \emptyset$ for $i \neq j$. Piecewise contractions have recently been used to study spiking neural networks (Catsigeras and Guiraud, to appear; Cessac, 2008). Piecewise contractive maps generate symbolic sequences by traversing the various partitions of the domain, yet they generally avoid chaotic regimes. Recently, several classes of piecewise contractive maps have proven to be generically asymptotically periodic and therefore nonchaotic (Bruin and Deane, 2009; Brémont, 2006; Catsigeras and Budelli, 2011). Counterexamples exist (Kruglikov and Rypdal, 2006), but this is the exception rather than the rule, as expansive dynamics are typically required in order to generate chaotic behavior. In our work, we extend the application of the theory of piecewise contractive mappings to single-neuron modeling. In doing so, we also shed new light on bursting phenomena in particular.

The remainder of this paper is organized as follows. In section 2, we formally introduce the model, provide its solution formula, and define the solutions considered in this study. In section 3.1, we reduce the model to a one-dimensional map, and in section 3.2, we discuss its piecewise contractive property. We show that piecewise contractive dynamics are an inherent property of this model, and we provide an analytical expression for the derivative of the map at every point. We use this analytical expression to conduct a numerical search of parameter values for which the model satisfies the piecewise contractive property. In section 4, we discuss tonic spiking in the model. We show that in the tonic firing regime, there is a one-to-one correspondence between the external inputs to a neuron and its asymptotic firing rate. We also provide a sufficient analytical condition on the parameters that ensures that the return map is globally contractive; in this case the neuron fires tonically. In section 5, we develop a generalization of bursting behaviors observed in our neurons that we call bursting maps. We show that bursting maps robustly generate periodic orbits with symbolic dynamics that are the simplest possible description of bursting phenomena. We discuss transitions between solution types under parameter variation, along with some associated issues of co-existence, in section 6. Finally, in section 7, we make concluding remarks, comment further on the relation of our work to some others in the literature, and point out directions for future research.

2. The neuron model

2.1. General model definition

The model neuron to be studied is described by the following set of differential equations:

$$I_j'(t) = -k_j I_j, j=1,\ldots,n, V'(t) = I_e + \sum_j I_j(t) - \gamma(V(t) - V_0), \quad (2.1)$$

where I_j are internal ("spike-induced") currents and $V(t)$ is the voltage. All other quantities are constants: I_e is the injected (input) current, k_j and γ are inverse time constants, and V_0 is the resting potential. We assume henceforth that the k_j are all distinct from each other and from γ.

When the voltage reaches threshold, $V(t) = \Theta$, the state variables are updated. The update rules are

$$I_j(t) \leftarrow R_j I_j + A_j, V(t) \leftarrow V_0, \quad (2.2)$$

where $V_0 < \Theta$ is the reset potential. Typically, $R_i \in \{0, 1\}$ for all spike-induced currents I_i. If $R_i = 0$, the value of I_i is reset to A_i after every spike. If $R_i = 1$, the value of I_i is incremented by A_i following each spike; we refer to such spike-induced currents as *additive current*. The system defined by (2.1) and (2.2) will be referred to in the rest of this work as "the model."

We note that the model is a special case of the generalized integrate-and-fire model introduced by Mihalas and Niebur (2009). In their model, the threshold is adaptive (our model is the special case $a = b = 0$ of their equation 2.1), the input current I_e can be time dependent, and there is no limit on the number of spike-induced currents. In addition, to simplify the notation, we have divided terms involving currents by the membrane capacitance C, have changed the units of current from charge per time to voltage per time, and have defined $\gamma = G/C$, which has units of inverse time.

2.2. Model solution and spike condition

We now give the analytical formulas for solutions to the model equations specified by (2.1) and discuss their immediate implications. The formulas we present are a special case of

those described in Mihalas and Niebur (2009). Since the dynamical matrix in (2.1) is triangular, the system's eigenvalues λ_i are simply the negative inverses of the distinct inherent time constants, $-k_1,\ldots,-k_n$, $-\gamma$. Therefore, there is a single, stable attractor towards which all trajectories will converge, and the trajectories are all sums of exponentials $e^{\lambda_i t}$. Specifically, the solution to (2.1) with initial conditions $(I_{10},\ldots, I_{n0}, V_0)$ is

$$I_j(t)=I_{j0}\exp(-k_j t), V(t)=V_0+\frac{I_e}{\gamma}+\sum_{j=1}^{n}\frac{I_{j0}\exp(-k_j t)}{\gamma-k_j}-\exp(-\gamma t)\left(\frac{I_e}{\gamma}+\sum_{j=1}^{n}\frac{I_{j0}}{\gamma-k_j}\right). \quad (2.3)$$

Despite the existence of an attractor, the reset conditions (2.2) allow the model to capture nontrivial behaviors associated with neurons if the spike condition $V(t) - \Theta = 0$ can be satisfied. The transformation $x = e^{-t}$ reduces the spike condition to the equation $D(x) \doteq V(x) - \Theta = 0$. The time of a spike resulting from a set of initial conditions can then be found by computing the solutions to the following equation:

$$D(x) \equiv V_0 - \Theta+\frac{I_e}{\gamma}+\sum_{j=1}^{n}\frac{I_{j0}}{\gamma-k_j}x^{k_j} - \left(\frac{I_e}{\gamma}+\sum_{j=1}^{n}\frac{I_{j0}}{\gamma-k_j}\right)x^{\gamma}=0. \quad (2.4)$$

Remark 1. *In the analysis of models with reset, we may think of time two different ways. To focus on the time from one spike to the next, it is convenient to think of time being reset to* 0 *after each spike. Alternatively, to consider a spike train including many spikes, it is helpful to think of time as always increasing, without reset. Our analysis takes the former perspective, which appears already in the transformation* $x = e^{-t}$ *and* (2.4). *In our figures, we follow the common convention of showing time increasing across multiple spikes, as in the second perspective.*

Writing the set of all real solutions to (2.4) as $\{x_1,\ldots, x_m\}$, the solution that corresponds to the first spike time is

$$x=\max\{x_i \in (0,1)\}. \quad (2.5)$$

If $D(x) = 0$ has no solution, the neuron will not spike. In the phase plane, this means that the system approaches a stationary state at which $V < \Theta$ and all state derivatives are zero. We can establish sufficient conditions for spiking to occur by evaluating $D(x)$ at the endpoints of the interval on which x is defined, $x = 0$ and $x = 1$:

$$D(0)=V_0 - \Theta+\frac{I_e}{\gamma}, D(1)=V_0 - \Theta. \quad (2.6)$$

Relevant parameter sets have $V_0 < \Theta$ such that $D(1)$ is negative, and thus a sufficient condition for a spike to occur, independent of $\{I_{j0}\}$, is

$$\frac{I_e}{\gamma} \geq \Theta - V_0. \quad (2.7)$$

If this condition is met, then by the intermediate value theorem $D(x)$ must have a root for some real $x \in (0, 1)$.

2.3. Simplified model and solution types

To facilitate the analysis of the asymptotic aspects of its dynamics, we define a simplified form of the model on which we will focus in this paper.

Definition 2.1. *The simplified model obeys* (2.1) *with reset conditions* (2.2) *and has the following properties*:

- **a.** $n = 2$ *(two internal currents)*;
- **b.** $R_1 = 1$, $R_2 = 0$ *(one additive current)*;
- **c.** $A_1 < 0$ *(the additive current is negative)*.

Positive additive currents tend to yield unstable dynamics, such as a firing rate that diverges to infinity over time, and they are not considered below. Henceforth, when we refer to (2.3) and (2.4), we mean the case where $n = 2$.

Remark 2. *Since there is only one current for which the reset depends on its value before a spike and we have fixed the threshold* Θ, *the model may be reduced to a one-dimensional map (see section* 3 *and beyond). If the threshold is not fixed, as in the general model, a two-dimensional map is needed to describe the dynamics even with a reset of just one current. Unfortunately, the study of two-dimensional maps using analytical tools is difficult, and their analysis typically requires numerical methods* (Shilnikov and Rulkov, 2003; Manica, Medvedev, and Rubin, 2010).

For model (2.1), we can distinguish various types of solutions, depending on the existence and patterns of spike threshold crossings. Recall that when a spike occurs, corresponding to (2.4) being satisfied, the reset conditions (2.2) are implemented, yielding new initial conditions in (V, I_1, I_2). Define an interspike interval as the time between two successive spikes.

Definition 2.2. *A quiescent solution is one that never reaches threshold. A phasic spiking or phasic solution is a solution for which, after finitely many spikes, a reset occurs after which no additional spikes occur*.

When a solution is neither quiescent nor phasic, it exhibits sustained spiking, meaning that the corresponding trajectory crosses threshold infinitely many times. Within the family of sustained spiking solutions, we distinguish two special types.

Definition 2.3. *A tonic spiking solution is a periodic solution in which all interspike times are equal. A bursting solution is a periodic solution for which the sequence of interspike intervals consists of subsequences of two or more consecutive small values alternating with individual large values*.

Remark 3. *The determination of what are small and large interspike intervals in the definition of a bursting solution is ambiguous. The neuroscience literature includes various algorithms for deciding whether a sequence of interspike intervals qualifies as a bursting solution or not. In section* 3, *we will provide a formulation that provides an unambiguous way to identify bursting solutions*.

If $R_1 = R_2 = 0$, the neuron will either fire tonically or will not fire at all, since the state variables will be reset to the same values after each spike. We shall see that with the restriction $R_1 = 1$, $R_2 = 0$, complex behaviors such as bursting can occur, as long as $A_1 < 0$, such that $I_1 < 0$. We consider tonic spiking and bursting solutions in sections 4 and 5,

respectively. In section 6, we discuss co-existence of solution types for fixed parameter sets and transitions between solutions as parameters are varied.

2.4. Implementation details

To reduce computation cost in simulations, the model's eigenvalues are typically chosen to be rational or integer multiples of each other, in which case (2.4) is a polynomial in x to a power, which can be solved using standard numerical techniques. To find the spike time, one must find the largest root of $D(x)$ in (0, 1). In Brette (2007), a hybrid bisection/Newton–Raphson method is proposed that solves this problem efficiently. The method relies on recursive bisection followed by the application of the method of Sturm sequences to find the exact number of roots in a given interval. To ease the computational burden this method entails, one can often discard the possibility of a spike using Descartes's rule of signs, which states that for an arbitrary polynomial

$$D(x)=a_n x^n+a_{n-1}x^{n-1}+\cdots+a_0, \quad (2.8)$$

the number of positive, real roots is equal to the number of sign changes in the sequence a_n, …, a_0 or is less than it by a multiple of 2. Denote the number of sign changes in the polynomial $D(x)$ by $\Delta(D(x))$. In the case of a constant threshold and two spike-induced currents, $\Delta(D(x)) \leq 3$. A sufficient condition for ruling out a spike from a particular set of initial conditions is that $\Delta(D(x)) = 0$, while $\Delta(D(x)) = 1$ or 3, which requires $D(0) > 0$, ensures that a spike occurs.

3. Return map properties

3.1. Map definition and basic structure

We henceforth consider only nonquiescent solutions. Recall that spike times are given as maximal solutions x to the spiking equation $D(x) = 0$, and these depend on the initial conditions. In general, we could write this equation as $D(x, I_{10}, I_{20}, V_0) = 0$, where ($I_{10}$, I_{20}, V_0) denote the values of our variables at time 0, to emphasize this point. Since we are considering only nonconstant resets for one internal current (I_1), however, we may express the spiking equation more simply as $D(x, I_{10}) = 0$ and view our model system as a *return map* or *Poincaré map* from the I_1 value immediately following one spike and reset to the I_1 value immediately following the next spike and reset. If the spike count is n, the return map is defined as

$$I_1^{n+1}=\Phi(I_1^n), \quad (3.1)$$

where we have shortened the subscript 10 to 1 for simplicity. The value of Φ is computed from the decay from the input value of the current up to the next spike time, followed by the addition of A_1 in the reset:

$$\Phi(I_1)=I_1 x^{k_1}+A_1, \quad (3.2)$$

where x depends implicitly on I_1 as defined by $D(x, I_1) = 0$, and $I_1 < 0$. Since $x > 0$, we have that $\Phi(I_1) \leq A_1$. The characteristics of the return map Φ fully specify the qualitative behavior of our model neurons. Examples of return maps for various spiking scenarios are shown in Figure 1; we discuss details of their classification below.

The return map Φ is piecewise continuous in a manner that we make precise in the following lemma. For the following analysis, it is critical that spike times be defined as maximal

solutions to $D(x, I_1) = 0$, but we will not explicitly include the max operation in writing this equation.

Lemma 3.1. *Given a neuron as defined in section* 2, *the map* $\Phi : \mathbb{R}^- \to \mathbb{R}^-$ *has either no discontinuities or one point of discontinuity, call it* I_d, *away from which* Φ *is differentiable. In the latter case,* Φ *experiences a downward jump at its discontinuity*: $\Phi(I_d^+) < \Phi(I_d^-)$.

Proof. By the implicit function theorem, the equation $D(x, I_1) = 0$ defines a differentiable function $x = f(I_1)$ on all open intervals where $D_x(x, I_1) \neq 0$. Hence, points I_1 for which $D_x(f(I_1), I_1) = 0$ represent the possible discontinuities of Φ as defined by (3.2), and Φ is differentiable away from such points. In fact, any points of discontinuity occur due to changes in the initial value of I_1 that cause $D(x, I_1)$ to gain or lose a root. (This phenomenon is illustrated in Figure 4(c) below.) Correspondingly, there are only two ways in which the solution $x = f(I_1)$, satisfying $D(x, I_1) = 0$, may experience a discontinuity as I_1 increases: either an existing maximal solution x_{max} disappears outside of the open interval (0, 1), or a new solution $x_{\tilde{max}}$ appears as I_1 is increased, such that $1 > x_{\tilde{max}} > x_{max}$, and the max operation in (2.5) will select the larger root $x_{\tilde{max}}$. In fact, the former case is impossible; an increase in I_1 can only make the neuron spike sooner. This is a simple consequence of the fact that $\frac{\partial V(t)}{\partial I_1} > 0$, which we prove in section 3.2. However, it is indeed possible for a larger solution x_{max} to appear as I_1 is increased, corresponding to a faster spike time. Therefore, $x(I_1)$ must experience an upward discontinuity in magnitude as I_1 increases if a discontinuity is experienced at all, and this change in x yields a downward jump in Φ, since $I_1 < 0$ by our general assumptions.

To see why Φ can have at most one discontinuity, consider that the voltage $V(t')$ at a fixed time t' increases monotonically with I_1. The solution x experiences a discontinuity when a local maximum of $V(t)$ is pushed above the threshold Θ as I_1 is increased. From (2.3), we see that the voltage $V(t)$ is a weighted sum of three exponentials. It follows that $V(t)$ contains at most two critical points and therefore at most one local maximum. Therefore, a local maximum of $V(t)$ can be pushed above the threshold Θ by increasing I_1 at most one time, proving that Φ has at most a single discontinuity.

Lemma 3.1 provides a natural way to define the bursting solutions introduced in Definition 2.3. Suppose Φ has a discontinuity. Since $\frac{\partial V(t)}{\partial I_1} > 0$, we can associate short times to spike with iterations on the larger I_1 component of Φ and long times to spike with iterations on the more negative I_1 component. A bursting solution is an orbit with subsequences of consecutive iterates on the short time component of Φ, interrupted by single iterates on the long time component.

3.2. Contraction and piecewise contraction

For general one-dimensional iterated maps, chaotic behavior of the iterations $\{I, \Phi(I), \Phi^2(I), \ldots\}$ can arise from very simple mapping functions Φ. On the other hand, a class of iterated maps known as contractive mappings always gives rise to simple dynamics.

Definition 3.2. *A function on a metric space* $f : S \to S$ *is a contractive mapping if there exists a constant* $r < 1$ *such that* $d(f(x), f(y)) \leq r d(x, y)$ *for all x and y in S.*

These maps are especially stable, as made precise by the following classical result.

Theorem 3.3 (contractive mapping principle). *If $f : S \to S$ is a contractive mapping and S is a complete space, there exists a unique fixed point x_0, and $x_0 = \lim_{n\to\infty} f^n(x)$ for any point $x \in S$.*

Proof. See Rudin (1976) or any introductory book on real analysis.

A consequence of Theorem 3.3 is that if $\Phi : \mathbb{R}^- \to \mathbb{R}^-$ is a contractive mapping on its entire domain, all of its orbits converge asymptotically to a unique, stable, fixed point I_{fix}. Another consequence of the theorem is that a fixed point I_{fix} of a differentiable map Φ is locally stable if there exists an epsilon-ball $B_\varepsilon(I_{fix})$ of the fixed point I_{fix} for which $\Phi(I) : B_\varepsilon(I_{fix}) \to B_\varepsilon(I_{fix})$ satisfies the contractive condition:

$$|\Phi'(I_1)| = \left|\frac{d\Phi(I_1)}{dI_1}\right| < 1. \quad (3.3)$$

Then, given any initial point $I_1 \in B_\varepsilon(I_{fix})$, its iterates will converge to I_{fix}.

Interestingly, most parameter choices used for simulations result in $\Phi(I_1)$ satisfying the piecewise contractive property, which we now define.

Definition 3.4. *The return map Φ of our model neuron is piecewise contractive if*

$$|\Phi'(I_1)| < \delta < 1 \quad (3.4)$$

on every open domain $D \subset \mathbb{R}^-$ such that $D \cap \{I_d\} = \emptyset$, where $\{I_d\}$ is the set of discontinuities of Φ.

Finding sufficient conditions on the parameters such that the piecewise contractive property holds requires finding analytical bounds for $|\Phi'|$. As we will show, this task is rather difficult. The quantity $|\Phi'|$ is related to the separation of nearby trajectories in the phase space in the I_1 direction. In continuous dynamical systems, the evolution of this separation over time is described by Lyapunov exponents. For the model we consider, however, a negative Lyapunov exponent does not guarantee the contractivity of Φ, because nearby trajectories will attain the spiking line $V(t) = \Theta$ at different times. The piecewise contractive property of Φ depends on the following: how is a small initial displacement δI_1 evolved along a trajectory from the reset line ($V = V_0$) to the spike line ($V = \Theta$)? If the end displacement is always smaller than the initial displacement, Φ is globally contractive. If this is the case only when the initial values of I_1 are on the same subset S_j, then Φ is piecewise contractive. A plot of a set of neighboring trajectories is shown in Figure 2(a) for the globally contractive case and in Figure 2(b) for the piecewise contractive case.

If we introduce a perturbation δI_1 to $I_1 = I_1(0)$, then we change the value of $I_1(t)$ along the solution as well as the time until the next spike. For two arguments of Φ given by $\tilde{I}_1 = I_1 + \delta I_1$ and I_1, yielding spike times $\tilde{t}$ and t, respectively, (2.3) gives

$$\Phi(\tilde{I}_1) - \Phi(I_1) = (I_1 + \delta I_1)\exp(-k_1\tilde{t}) - I_1\exp(-k_1 t).$$

For parameters leading to biologically relevant spiking patterns, small perturbations δI_1 typically result in negligible differences in spike times, $\tilde{t} \approx t$. This occurs since the external current I_e is typically the main driving force of the neuron and hence is the main contributor to the spiking rate. Thus, to leading order, $\Phi(\tilde{I}_1) - \Phi(I_1) \approx \delta I_1 \exp(-k_1 t)$, and locally contractive dynamics appear to be an inherent property of neurons defined in section 2.

To construct an exact condition for the piecewise contractive property to hold at a given point I_1, we compute the derivative of the return map from (3.2):

$$\Phi'(I_1)=x^{k_1}+k_1 I_1 x^{k_1-1}\left(\frac{dx}{dI_1}\right). \quad (3.5)$$

We compute an implicit expression for $\frac{dx}{dI_1}$ by invoking the implicit function theorem, which states that for any open domain in which $\frac{\partial D(x,I_1)}{\partial x} \neq 0$, the following holds:

$$\frac{dx}{dI_1}=-\left(\frac{\partial D(x,I_1)}{\partial I_1}\right)\left(\frac{\partial D(x,I_1)}{\partial x}\right)^{-1}. \quad (3.6)$$

The numerator of this expression is positive, since

$$\frac{\partial D(x,I_1)}{\partial I_1}=\left(\frac{1}{\gamma-k_1}\right)(x^{k_1}-x^{\gamma})>0 \quad (3.7)$$

for $x \in (0, 1)$. The denominator must be negative, since $\frac{\partial V(t)}{\partial t}>0$ must hold at the moment the neuron spikes, and therefore

$$\frac{\partial D(x,I_1)}{\partial x}=\left(\frac{\partial D(x,I_1)}{\partial t}\right)\left(\frac{\partial t}{\partial x}\right)<0. \quad (3.8)$$

The above equations prove that

$$\frac{dx}{dI_1}>0. \quad (3.9)$$

This result is intuitive, because an increase in I_1 results in a monotonic increase in the derivative of the voltage $V'(\tilde{t})$ at any fixed $\tilde{t}$. Hence the neuron spikes sooner for larger values of I_1, leading to a larger solution $x = e^{-t}$ to $D(x, I_1) = 0$. It then follows from (3.5) that

$$1>x^{k_1}>\Phi'(I_1) \quad (3.10)$$

for all $I_1 \in \mathbb{R}^-$. After some algebraic manipulation, one obtains

$$\Phi'(I_1)=x^{k_1}\left(1-\frac{k_1 I_1\left(\frac{1}{\gamma-k_1}\right)(x^{k_1}-x^{\gamma})}{I_1\left(\frac{1}{\gamma-k_1}\right)(k_1 x^{k_1}-\gamma x^{\gamma})+I_2\left(\frac{1}{\gamma-k_2}\right)(k_2 x^{k_2}-\gamma x^{\gamma})-I_e x^{\gamma}}\right). \quad (3.11)$$

If the right-hand side of (3.11) has a value greater than −1 for all $I_1 \in \mathbb{R}^-$, the contractive property holds in this domain. For parameters leading to biologically relevant spiking behaviors such as tonic spiking and bursting, including the parameter choices discussed in this paper as well as in Mihalas and Niebur (2009), this condition typically holds.

In section 4.2 we use (3.11) to obtain a condition on the parameters to ensure globally contractive behavior in the case that $I_2 = 0$. Since we did not find a simple analytical condition to ensure contractive behavior for $I_2 \neq 0$, we performed a numerical exploration of parameter space using MATLAB. At every permutation of the parameter values shown in Table 2, the largest root of $D(x)$ in (0, 1) was computed using the MATLAB roots function,

and this x value was used in (3.11) to verify the contractive condition. The lowest derivative was found to be −0.39. This allows a significant margin of error for the map's derivative at values of I_1 in between those values at which the condition was checked. In particular, we observed that increasing I_e stabilizes the dynamics. This is not surprising, since at any fixed value of I_1, in the $I_e \to \infty$ limit, $x \to 1$ and $\Phi'(I_1) \to 1$.

An example of an expansive (noncontractive) return map is shown in Figure 1(f). This map generates period-2 oscillations. On the other hand, such oscillations can also be generated by piecewise contractive maps such as that shown in Figure 1(e). In this study, we shall focus on the case when Φ is contractive or piecewise contractive, since this is the predominant case arising in our model over a broad range of parameter values, such as those shown in Table 2.

4. Tonic spiking

4.1. Uniqueness of the fixed point

Tonic spiking solutions correspond to fixed points of the return map $\Phi(I_1)$. These fixed points occur at values of I_1 for which

$$\Phi(I_1)=I_1x^{k_1}+A_1=I_1. \quad (4.1)$$

In a plot of $\Phi(I_1)$, fixed points occur when the return map intersects the $\Phi(I_1) = I_1$ line, as shown in Figures 1 and 3.

Lemma 4.1. *The return map* Φ(*I*) *for the model neuron described in section* 2 *contains at most one fixed point.*

Proof. We prove this result by contradiction. Assume there are two fixed points I_1 and I_2 in $(-\infty, 0]$. If both of these points belong to the same interval S_j, then the map $\Phi(I_1)$ is continuous in the interval (I_1, I_2). As established in Lemma 3.1, Φ is also differentiable in this interval. By the mean value theorem, there must therefore be a point $I_1 < I' < I_2$ at which

$$\Phi'(I')=\frac{\Phi(I_2)-\Phi(I_1)}{I_2-I_1}=1. \quad (4.2)$$

However, we have that $1 > x^{k1} > \Phi'(I_1)$ from (3.10). Therefore, there cannot be two fixed points in the interval. On the other hand, suppose fixed points I_1 and I_2 belong to separate intervals S_1 and S_2 separated by the discontinuity point I_d. Since $I_d > I_1$, $\Phi(I_1) = I_1$, and $\Phi' < 1$, we have $\lim_{I\to I_d^-}\Phi(I)<I_d$. By Lemma 3.1, Φ experiences a downward discontinuity at I_d, and hence there exists a sufficiently small ε for which $\Phi(I_d + \varepsilon) < I_d$. Since $I_d + \varepsilon$ and I_2 both belong to S_2, there exists a point $I_d + \varepsilon < I' < I_2$ at which

$$\Phi'(I')=\frac{\Phi(I_2)-\Phi(I_d+\varepsilon)}{I_2-(I_d+\varepsilon)}>\frac{I_2-I_d-\varepsilon}{I_2-I_d-\varepsilon}=1. \quad (4.3)$$

This concludes the proof.

We have already seen that under condition (2.7), quiescent solutions do not exist. The consequence of Lemma 4.1 is that for a fixed parameter set, the neuron may exhibit periodic tonic spiking at only one frequency. Local stability of the associated fixed point is guaranteed for maps satisfying the piecewise contractive property as long as the fixed point I_{fix} is a positive distance d_0 from the discontinuity set $\{I_d\}$. If (2.7) holds, then Lemma 4.1

implies that bistability or hysteresis in the model can occur only if it involves aperiodic or bursting states.

4.2. A sufficient condition for tonic spiking

If Φ is globally contractive on $\mathbb{R}^-$ and has no discontinuity points, all orbits approach a tonic spiking state. This follows directly from Theorem 3.3. A differential-geometric approach to finding sufficient contractive conditions on the parameters for a two-dimensional spiking neuron model is developed by Foxall et al. (2012). The subthreshold dynamics of the class of two-dimensional systems considered in that study are nonlinear and do not generally admit analytical solutions. In contrast, in our case, we may use the analytical solution of the subthreshold dynamics to derive a sufficient condition for contractive behavior and hence tonic spiking.

If we consider model neurons in which $I_2 = 0$, thus restricting our analysis to a two-dimensional model, the following simple contractive condition exists.

Proposition 4.2. *Consider a neuron with* $I_2 = 0$. *If* $k_1 > 2\gamma$ *and*

$$I_e > \frac{k_1(\Theta - V_0)}{2}, \quad (4.4)$$

then Φ *is contractive for* $I_1 \in \mathbb{R}^-$ *and all orbits converge to a tonic spiking state*.

Proof. Note that under the conditions of the proposition, (2.7) holds, and thus the neuron spikes repetitively. We now establish the contractive property, which ensures convergence to a periodic tonic state. By rewriting (3.11) as

$$\Phi'(I_1) = x^{k_1}\left(1 - \frac{g(x, I_1)}{h(x, I_1)}\right) \quad (4.5)$$

and recalling (3.10), we see that $2 > \frac{g(x, I_1)}{h(x, I_1)}$ ensures that $|\Phi'(I_1)| < 1$. We also recall that $g(x, I_1)$ and $h(x, I_1)$ are both negative by preceding arguments. Therefore, a contractive condition is that $g(x, I_1) > 2h(x, I_1)$. We now set $I_2 = 0$ in (3.5) and in (2.4). The latter equation allows us to cancel the x^{k1} terms in favor of x^γ terms. This yields

$$h(x, I_1) = k_1\left(\Theta - V_0 - \frac{I_e}{\gamma} + \frac{I_e}{\gamma}x^\gamma\right) - (I_e + I_1)x^\gamma, \; g(x, I_1) = k_1\left(\Theta - V_0 - \frac{I_e}{\gamma} + \frac{I_e}{\gamma}x^\gamma\right). \quad (4.6)$$

Writing the contractive condition $g(x, I_1) > 2h(x, I_1)$ and simplifying, we obtain

$$x^\gamma\left[I_e\left(2 - \frac{k_1}{\gamma}\right) + 2I_1\right] > k_1\left(-\frac{I_e}{\gamma} + \Theta - V_0\right). \quad (4.7)$$

The proposition then follows from $1 > x^\gamma > 0$ and some simple algebraic manipulation. Note that we used $k_1 > 2\gamma$ to ensure that the left-hand side of (4.7) is negative for all values of $I_1 \in \mathbb{R}^-$.

A consequence of Proposition 4.2 is that for model neurons for which $I_2 = 0$ and $k_1 > 2\gamma$, there always exists I_{min} such that $\Phi(I_1)$ is globally contractive on $\mathbb{R}^-$ for all $I_e > I_{min}$. Thus, increasing the external current has a stabilizing effect on the dynamics of these neurons. One can always make these neurons fire tonically by setting I_e to be sufficiently large. We note

that a very similar result was obtained by Touboul and Brette (2009) for a nonlinear spiking model.

5. Bursting

5.1. Phase space analysis

We now analyze the bursting scenario in the phase plane. This analysis will allow us to derive necessary conditions for bursting and also provides an algorithm for generating parameters that lead to bursting.

As introduced in section 3.1, bursting can occur when $\Phi(I_1)$ experiences a downward discontinuity at a discontinuity point I_d. This discontinuity can cause the iterates of Φ to follow a cyclic pattern along which it visits both components of Φ, as seen in the cobwebs in Figures 1(d) and 1(e). The discontinuity of Φ occurs at the value of I_1 at which $V'(t(I_1)) = 0$ and $V''(t(I_1)) < 0$, where $t(I_1)$ is the spike time. At this location, an infinitesimal change to the value I_1 will cause the trajectory to miss the spiking surface, resulting in a discontinuous change in the timing of the spiking event. This situation is observed in Figure 2(b) and is referred to as a *grazing bifurcation* by some authors (e.g., Donde and Hiskens, 2004).

At a grazing bifurcation, the following equations are satisfied:

$$V(t)=\Theta>V_0, \quad (5.1)$$

$$\frac{dV(t)}{dt}=I_e+I_1(t)+I_2(t)-\gamma(V(t)-V_0)=0, \quad (5.2)$$

$$\frac{d^2V(t)}{dt^2}=-k_1I_1(t)-k_2I_2(t)-\gamma\left(\frac{dV(t)}{dt}\right)=-k_1I_1(t)-k_2I_2(t)<0, \quad (5.3)$$

where we used (2.3) to compute (5.2), and we used (5.2) to obtain (5.3). We now show that such an event can occur only if condition (2.7) is satisfied, and we subsequently assume that it holds.

Proposition 5.1. *Condition* (2.7) *is necessary for the existence of a bursting solution*.

Proof. Recall that $D(1) < 0$, independent of I_1. For a bursting solution to exist, there must be a value I_1 such that a grazing bifurcation occurs at some $x_g \in (0, 1)$ and a later spike occurs at some $x_s \in (0, x_g)$. A grazing bifurcation represents a multiplicity two root of $D(x) = 0$, while the later spike corresponds to an additional root. If condition (2.7) does not hold, then $D(0) < 0$, so $D(x)$ must have yet another root in $(0, x_s)$. But with $n = 2$, the polynomial $D(x)$ is given by a constant plus three x-dependent terms and thus cannot have four positive real roots (counting multiplicities).

From (2.7), (5.1), and (5.2), we have

$$I_1(t)+I_2(t)=\gamma(\Theta-V_0)-I_e<0. \quad (5.4)$$

From (5.3), we also have that

$$k_1I_1(t)+k_2I_2(t)>0. \quad (5.5)$$

Recall that $I_1(t) < 0$ and $I_2(t) > 0$. It follows that (5.4) and (5.5) can never be mutually satisfied if $k_1 > k_2$. Thus, the following is a necessary condition for bursting:

$$k_2 > k_1. \quad (5.6)$$

The following algorithm provides a practical method for finding bursting parameters by constructing a grazing bifurcation:

1. Choose some V_0, I_e, I_{10}, I_{20}, γ, k_1, k_2 such that $I_e > 0$, $I_{10} < 0$, $I_{20} > 0$, $I_{10} + I_{20} = 0$, and $k_1 = k_2 > 0$. For any t, the following equations hold:

$$I_1(t) + I_2(t) = 0, \quad (5.7)$$

$$k_1 I_1(t) + k_2 I_2(t) = 0, \quad (5.8)$$

$$\gamma(V(t) - V_0) - I_e = -I_e \exp(-\gamma t), \quad (5.9)$$

where the last equation follows from the model solutions in (2.3). As a trivial consequence,

$$\gamma(V(t) - V_0) - I_e < I_1(t) + I_2(t) \quad (5.10)$$

such that (5.4) cannot be satisfied for any $t > 0$.

2. Now choose $t = t_1$ such that $t_1 k_2 < 1$. This choice ensures that

$$\frac{\partial}{\partial k_2}(k_2 \exp(-k_2 t_1)) = (1 - t_1 k_2)\exp(-k_2 t_1) > 0. \quad (5.11)$$

Keeping the same values of the time constants, we now compute the margin of (5.10):

$$\alpha_0 = I_{10}\exp(k_1 t_1) + I_{20}\exp(k_2 t_1) - \gamma(V(t_1) - V_0) + I_e \quad (5.12)$$

$$= I_e \exp(-\gamma t_1) > 0. \quad (5.13)$$

3. Find a perturbation $\Delta k_2 > 0$ such that the following equations are satisfied:

$$k_1 I_{10}\exp(-k_1 t_1) + (k_2 + \Delta k_2) I_{20}\exp(-(k_2 + \Delta k_2)t_1) > 0, \quad (5.14)$$

$$I_{10}\exp(-k_1 t_1) + I_{20}\exp(-(k_2 + \Delta k_2)t_1) > \gamma(V(t_1, k_2 + \Delta k_2) - V_0) - I_e, \quad (5.15)$$

where we have written $V(t_1, k_2 + \Delta k_2)$ to make the dependence of the voltage on the current k_2 explicit. From (5.11), we see that (5.14) is satisfied for any

$$\Delta k_2 < \frac{1}{t_1} - k_2. \quad (5.16)$$

Equation (5.15) is satisfied for sufficiently small Δk_2, since the left-hand side of (5.10) increases monotonically with k_2 and the right-hand side decreases monotonically with k_2. Once a suitable Δk_2 is found, we set

$$k_2^{'}=k_2+\Delta k_2. \quad (5.17)$$

This new time constant ensures that inequality (5.5) will be satisfied at $t = t_1$. This will give us the negative second derivative that is needed to induce a grazing bifurcation.

4. Compute the margin of inequality (5.15) at $t = t_1$ using $k_2^{'}$ instead of $k_2 + \Delta k_2$:

$$\alpha_1=I_{10}\exp(k_1t_1)+I_{20}\exp(k_2^{'}t_1)-\gamma(V(t_1,k_2^{'})-V_0)+I_e>0. \quad (5.18)$$

We will now decrease I_e in such a way that the V-nullcline equation (5.2) will be satisfied at $t = t_1$. From the solution formulas (2.3) we have that

$$\frac{\partial[\gamma(V(t)-V_0)-I_e]}{\partial I_e}=-\exp(-\gamma t)<0. \quad (5.19)$$

Using this equation, we find the external current that reduces the margin in inequality (5.10) to zero, which results in the V-nullcline equation being satisfied at $t = t_1$:

$$I_e^{'}=I_e-\alpha_1\exp(\gamma t_1). \quad (5.20)$$

From this choice and (5.12) we have that $\alpha_0 > \alpha_1$. Hence, we have

$$I_e^{'}>I_e-\alpha_0\exp(\gamma t_1)=0. \quad (5.21)$$

This condition guarantees that

$$\left.\frac{dV(t)}{dt}\right|_{t=0}=\frac{I_e^{'}}{\gamma}>0, \quad (5.22)$$

which in turn yields $V(t_1,I_e^{'})>V_0$ (recall that $V(t)$ may have only two critical points, since it is the sum of three exponentials).

5. Finally, set

$$\Theta=V(t_1,I_e^{'},k_2^{'}). \quad (5.23)$$

We have now obtained parameters t_1, k_1, $k_2^{'}$, I_{10}, I_{20}, I_e, V_0, Θ that lead to a bursting-inducing grazing bifurcation at $t = t_1$.

The main results of this section are summarized in the following proposition.

Proposition 5.2. *Assume that* (2.7) *holds. Given any* I_{10}, k_1, γ, V_0, *at least one grazing bifurcation occurs in the region of parameter space specified by*

$$t\in\mathbb{R}^+,\ I_{20}\in\mathbb{R}^+,\ k_2\in(k_1,\infty),\ \Theta\in(V_0,\infty),\ I_e\in(\gamma(\Theta-V_0),\gamma(\Theta-V_0)+|I_{10}|),$$

and none occurs outside of this region.

Proof. The algorithm above serves as a constructive proof that this region of parameter space must contain at least one grazing bifurcation. On the other hand, we have also

observed in (5.6) that grazing bifurcations are impossible whenever $k_2 \le k_1$. The lower bound on I_e stems from (5.4), and the upper bound stems from the fact that at the bifurcation point,

$$I_e+I_{10}\exp(-k_1 t)+I_{20}\exp(-k_2 t)-\gamma(\Theta-V_0)=0,\ I_e+I_{10}\exp(-k_1 t)-\gamma(\Theta-V_0)<0,\ I_e<|I_{10}|+\gamma(\Theta-V_0), \quad (5.24)$$

thus completing the proof.

Of course, to obtain bursting behavior in the model, appropriate values of the reset parameters A_1, A_2 are needed. To obtain bursting dynamics from a grazing bifurcation constructed as in the above algorithm, we set $A_2 = I_{20}$ and then adjust the height of the map using A_1 to ensure that the fixed point line $\Phi(I) = I$ intersects neither the left nor the right part of the map, as shown in Figure 4(b).

5.2. Bursting maps

As described above, Φ contains at most a single fixed point and at most a single discontinuity. If there is no fixed point, then the neuron may burst or display nonperiodic behavior. We shall show that the following class of maps robustly generates bursting-like behavior.

Definition 5.3. *The return map Φ for a model neuron is a bursting map if it is piecewise contractive with a point of discontinuity $I_d < 0$ and there exist some $\varepsilon_1, \varepsilon_2 > 0$ for which the following conditions hold*:

$$\Phi(I) - I > \varepsilon_1 \text{ for } I \in (-\infty, I_d),\ I - \Phi(I) > \varepsilon_2 \text{ for } I \in [I_d, 0]. \quad (5.25)$$

We note that periodic solutions occurring in maps with a single discontinuity are also discussed in Hogan, Higham, and Griffin (2007). We also note that this definition can be applied to return maps of an adaptation variable generated by models other than that defined in section 2. In order for the results that follow to apply to other models, however, it is crucial that the spike times depend monotonically on the value of the adaptation variable. This condition is satisfied for maps $\Phi(I)$ generated from our model, since as shown in section 3.2 we have $\frac{dt_{sp}}{dI} < 0$ for all $I \in \mathbb{R}$, where t_{sp} is the time of the next spike.

Not all piecewise contractive maps generated by our model neurons will satisfy the conditions of a bursting map. However, note that the parameter A_1 affects solely the height of the map and has no effect on the map's derivative at any point, as can be seen from (3.2). Since Φ experiences a downward discontinuity at I_d (Lemma 3.1), given model parameters $\vec{p} \in (I_e, V_0, \Theta, I_{20}, \gamma, k_1, k_2)$ that generate a piecewise contractive map, one can always find $A_1 \in \mathbb{R}^-$ such that the conditions of a bursting map are satisfied.

An example of a bursting map is shown in Figures 4(a)–4(c). We observe numerically that such maps are preperiodic: the orbits of the map robustly tend to a periodic pattern regardless of initial conditions. In this section, we provide mathematical justification for the observed bursting behaviors. Our approach draws on the work by Gambaudo and Tresser (1988) and Brémont (2006).

The discontinuity in Φ complicates the application of the contraction principle but does not prohibit its use. Since the map is discontinuous at I_d, there always exist $x, y \in \mathbb{R}^-$ such that $d(\Phi(x), \Phi(y)) > rd(x, y)$ for any value of r, as we may choose x and y to be arbitrarily close to the discontinuity point but on opposite sides. Therefore, $\Phi(I) : \mathbb{R}^- \to \mathbb{R}^-$ is not a contractive mapping, and we cannot directly apply the contractive mapping principle. Nevertheless, if

we can find a subset $V \subset \mathbb{R}^-$ such that $\Phi^m : V \to V$ continuously, then Φ^m is indeed a contraction on V. This follows from applying the chain rule to successive mappings and using piecewise contractivity:

$$\left|\frac{d\Phi^m(I)}{dI}\right| = \left|\frac{d\Phi^m(I)}{d\Phi^{m-1}(I)} \cdot \frac{d\Phi^{m-1}(I)}{d\Phi^{m-2}(I)} \cdot \cdots \cdot \frac{d\Phi(I)}{dI}\right| \quad (5.26)$$

$$= \prod_{n=0}^{n=m-1} \left|\frac{d\Phi(I_n)}{dI_n}\right| < 1, \quad (5.27)$$

where $I_{n+1} = \Phi(I_n)$. Therefore, $\Phi^m(I)$ may be a contractive mapping when I is restricted to the subset V. In this case, the map $\Phi^m : V \to V$ must contain a unique fixed point $I_{fix} \in V$ to which orbits in V converge. As we shall see, there may be several invariant sets V_i and periodicities m for a bursting map Φ.

5.3. Restriction of the domain to reachable sets

We define the notion of reachable sets. This notion allows us to restrict the action of Φ to a compact set R. An illustration of reachable sets is shown in Figure 5.

Definition 5.4. *Given a bursting map $\Phi : \mathbb{R}^- \to \mathbb{R}^-$, partition the domain $\mathbb{R}^-$ into the sets $S_0 = (-\infty, I_d)$ and $S_1 = [I_d, 0]$. We define the left and right reachable sets R_0 and R_1, respectively, and their union as follows*:

$$R_0 = [\min(\Phi(S_1)), I_d), \; R_1 = [I_d, \max(\Phi(S_0))], \; R = R_0 \cup R_1. \quad (5.28)$$

The reachable sets cover all points reachable from the opposite site of the discontinuity. Both sets must be nonempty; otherwise, $\Phi(S_i)$ maps S_i, $i \in \{0, 1\}$, continuously into itself, and Φ has a fixed point, which violates the definition of a bursting map. Note that R_0 and R_1 are bounded sets with finite measure, due to the boundedness of S_1.

We next prove an important preliminary result about the action of bursting maps on $\mathbb{R}^-$ and on R

Lemma 5.5. *Given a bursting map Φ, for each $I \in \mathbb{R}^-$, there exists i such that $\Phi^i(I) \in R$. Furthermore, $\Phi(R) \subset R$.*

Proof. On S_0 and hence on R_0, the map is increasing, in the sense that for $I \in S_0$,

$$I < \Phi(I) - \varepsilon_1 < \Phi^2(I) - 2\varepsilon_1 < \cdots. \quad (5.29)$$

The monotonic, increasing sequence $\{\Phi^i(I)\}$ will exceed I_d and thus reach S_1 in a finite number of iterations. Therefore, the orbit must eventually leave S_0 and reach R_1. Similar considerations hold for S_1. That $\Phi(R) \subset R$ follows directly from the construction of R.

Note that Lemma 5.5 does not imply the existence of a fixed point of Φ in R, since $\Phi : R \to R$ is not a continuous mapping.

The consequence of Lemma 5.5 is twofold. First, it allows us to consider a map that is defined on the compact set R, ignoring the part of the domain that is disjoint with R. Second, it implies that successive iterates of Φ are nested:

$$R \supset \Phi(R) \supset \Phi^2(R) \supset \Phi^3(R) \supset \cdots.$$

Therefore, if there indeed exists a periodic orbit $\{I_0, \Phi(I_0), \Phi^2(I_0), \ldots, I_0\}$, the following is evidently also true:

$$\{I_0, \Phi(I_0), \Phi^2(I_0), \ldots, I_0\} \subset \Phi^\infty(R),$$

where $\Phi^\infty(R)$ is a set of measure zero, due to the contractive condition. Such sets are more commonly known as ω-limit sets.

Definition 5.6. *The an ω-limit set ω(I) of a point I is the set of limit values of all convergent subsequences extracted from its forward orbit. More precisely, if* $p \in \omega(I)$*, then for any* $\varepsilon > 0$ *and* $m > 0$*, there exists* $n > m$ *such that* $d(\Phi^n(I), p) < \varepsilon$.

The definition of an ω-limit set extends naturally to intervals within the domain of Φ. A periodic point *x* must lie inside the ω-limit set of *R*.

As we shall see, injectivity of Φ simplifies the description of the genericity of asymptotically periodic dynamics. In our case, although bursting maps are generally not injective everywhere on $\mathbb{R}^-$, we can often find a *refined reachable set* $R' \subseteq R$ for which $\Phi : R' \to R'$ is injective. We now define this notion.

Definition 5.7. *Given a bursting map* Φ *with reachable set R, a refined reachable set is an interval that satisfies the following*:

- **a.** $\Phi(R') \subset R'$;
- **b.** $\Phi^n(R) \subset R'$ *for some* $n > 0$.

If a refined reachable set exists on which Φ is injective, all orbits will be attracted to it, and we may restrict our attention to the injective map $\Phi : R' \to R'$. The following lemma provides a sufficient condition for the injectivity of Φ on such a set *R*′.

Lemma 5.8. *Consider a bursting map* Φ *that is piecewise injective on R (it is injective on the reachable sets* R_0 *and* R_1*). Then, there exists a refined reachable set* $R' \subset R$ *for which the map* $\Phi : R' \to R'$ *is injective*.

Proof. We prove the lemma by considering the following three cases. The construction of the refined reachable sets for Cases I and II is illustrated in Figure 6.

- *Case* I: $\Phi' > 0$ on R_0 and R_1.

  We define the refined reachable sets as follows:

  $$R_0' = [\min(\Phi(R_1)), I_d), \; R_1' = [I_d, \max(\Phi(R_0))], \; R' = R_0' \cup R_1'. \quad (5.30)$$

  R′ satisfies the conditions of a refined reachable set. Indeed, suppose there exist $I_0 \in R_0', I_1 \in R_1'$ for which $\Phi(I_0) = \Phi(I_1)$. By the positivity of Φ′, the refined reachable sets are as follows:

  $$R' = [\Phi(I_d^+), \Phi(I_d^-)] = R_0' \cup R_1'. \quad (5.31)$$

  Applying the contraction hypothesis, we obtain

$$d(I_0, I_d) > d(\Phi(I_0), \Phi(I_d^-)) = |R_1'| \pm d(I_d, \Phi(I_0)),\ \ d(I_1, I_d) > d(\Phi(I_1), \Phi(I_d^+)) = |R_0'| \mp d(I_d, \Phi(I_1)), \quad (5.32)$$

where the signs in these equations depend on whether $\Phi(I_0) = \Phi(I_1)$ belongs to R_0 or to R_1. Adding these terms, we obtain

$$d(I_0, I_d) + d(I_1, I_d) > |R_0'| + |R_1'|, \quad (5.33)$$

which contradicts the fact that $d(I_0, I_d) < |R_0'|$ and $d(I_1, I_d) < |R_1'|$.

- *Case* II: $\Phi' > 0$ on R_i, $\Phi' < 0$ on R_{1-i} for some $i \in \{0, 1\}$.

  We consider the case that $i = 0$, as the case where $i = 1$ is similar. We construct the refined reachable sets as follows:

$$R_0' = [\Phi^2(I_d^-), I_d),\ \ R_1' = [I_d, \Phi(I_d^-)],\ \ R' = R_0' \cup R_1'. \quad (5.34)$$

  Again, it is easy to check that R' satisfies the requirements of a refined reachable set. If instead there exist $I_0 \in R_0', I_1 \in R_1'$ for which $\Phi(I_0) = \Phi(I_1)$, then the contraction hypothesis yields

$$d(I_0, I_d) > d(\Phi(I_0), \Phi(I_d^-)),\ \ d(I_1, \Phi(I_d^-)) > d(\Phi(I_1), \Phi^2(I_d^-)). \quad (5.35)$$

  Adding these terms using $\Phi(I_0) = \Phi(I_1)$, we obtain

$$d(I_0, I_d) + d(I_1, \Phi(I_d^-)) > |R'| = |R_0'| + |R_1'|, \quad (5.36)$$

  which contradicts the fact that $d(I_0, I_d) < |R_0'|$ and $d(I_1, \Phi(I_d^-)) < |R_1'|$.

- *Case* III: $\Phi' < 0$ on R_0 and R_1.

  We define the refined reachable set $R' = R$. The fact that Φ is injective on R' follows immediately from the fact that the map experiences a downward discontinuity at I_d. This concludes the proof.

The consequence of this lemma is that piecewise injectivity on $R \Rightarrow$ injectivity on a refined reachable set R'. Due to the complexity of the expression for the map's derivative in (3.11), we were unable to provide bounds on the parameters that indicate when Φ is piecewise injective on R. On the other hand, the return maps we have observed—including those in this paper—typically feature piecewise injectivity on R.

5.4. Periodic orbits

We now describe the periodic orbits that may arise from bursting maps. The following theorem is due to Gambaudo and Tresser. Our proof follows along the same lines as the proof found in Gambaudo and Tresser (1988) but also supplies some missing steps. An illustration of the proof is shown in Figure 7.

Theorem 5.9. *Recalling that Φ is right continuous, we denote*

$$\Phi(I_d^+) = \lim_{I \to I_d^+} \Phi(I) = \Phi(I_d)$$

and

$$\Phi(I_d^-) = \lim_{I \to I_d^-} \Phi(I).$$

With this notation,

$$\omega(R) = \omega(\Phi(I_d^+)) \cup \omega(\Phi(I_d^-)). \quad (5.37)$$

Proof. Suppose we are given a point $y \in R$. By comparing the orbit of y with the orbits of $\Phi(I_d^+)$ and $\Phi(I_d^-)$ simultaneously, we shall show that the ω-limit set of y must lie in the ω-limit set of either $\Phi(I_d^+)$ or $\Phi(I_d^-)$.

Suppose Φ has a (piecewise) Lipschitz constant $0 \le K < 1$. We first claim that for any $n > 0$, there exist $m_n \ge 0$ and $s_n \in \{+, -\}$ such that $d(\Phi^n(y), \Phi^{m_n}(I_d^{s_n})) \le K^n d(y, I_d)$. To show this, suppose $y \in R_i$, where $i \in \{0, 1\}$, and pick $s_1 = -$ (+) if $i = 0$ (1), which implies

$$d(\Phi(y), \Phi(I_d^{s_1})) \le K d(y, I_d). \quad (5.38)$$

Find $n = \min\{p \in \mathbf{N} : \Phi^p(y) \in R_i \text{ and } \Phi^p(I_d^{s_1}) \in R_j \text{ for } i, j \in \{0, 1\}, j \ne i\} \ge 1$. If $n > 1$, then the fact that $\Phi^{n-1}(y), \Phi^{n-1}(I_d^{s_1}) \in R_i$ for some fixed $i \in \{0, 1\}$ yields

$$d(\Phi^n(y), \Phi^n(I_d^{s_1})) \le K^n d(y, I_d); \quad (5.39)$$

that is, we can choose $s_q = s_1$ for $q = 1, \ldots, n$.

Suppose $\Phi^n(y) \in R_j$, $j \in \{0, 1\}$. We now choose $s_{n+1} \in \{+, -\}$ such that $\Phi(I_d^{s_{n+1}}) \in R_j$. Note that

$$d(\Phi^n(y), I_d) \le d(\Phi^n(y), \Phi^n(I_d^{s_1})), \quad (5.40)$$

since $\Phi^n(y)$ and $\Phi^n(I_d^{s_1})$ are on opposite sides of I_d (with equality if $I_d^{s_1} = I_d$). This is observed in Figure 7(a), where for $n = 1$ we have that $\Phi^n(y)$ and $\Phi^n(I_d^+)$ are on opposite sides of I_d. Thus, combining either (5.38), if $n = 1$, or (5.39) together with (5.40), a subsequent iterate gives

$$d(\Phi^{n+1}(y), \Phi(I_d^{s_{n+1}})) \le K d(\Phi^n(y), I_d) \le K^{n+1} d(y, I_d);$$

that is, we can take $m_{n+1} = 1$. Continuing this process and increasing n, we can monotonically decrease the distance between $\Phi^n(y)$ and $\Phi^{m_n}(I_d^{s_n})$, where the s_n and m_n depend on n. The contraction between the orbit of $I_d^{\pm}$ and of y is illustrated in Figures 7(b) and 7(c).

For any $\varepsilon > 0$, there exists an $N(\varepsilon)$ such that $d(\Phi^n(y), \Phi^{m_n}(I_d^{s_n})) \le \varepsilon/2$ for any $n > N(\varepsilon)$. Given a point $z \in \omega(y)$ and $\varepsilon > 0$, by definition there exists an infinite, increasing sequence of integers $\{n_i\}$ such that $n_i > N(\varepsilon)$ and

$$d(z, \Phi^{n_i}(y)) \le \varepsilon/2 \quad (5.41)$$

for all i. Then, by the triangle inequality,

$$\varepsilon \geq d(\Phi^{n_k}(y), \Phi^{m_{n_k}}(I_d^{s_{n_k}})) + d(z, \Phi^{n_k}(y)) > d(z, \Phi^{m_{n_k}}(I_d^{s_{n_k}})), \quad (5.42)$$

where the m_{n_k} that satisfy this equation must exist and are chosen as described above. Since each $s_{n_k} \in \{+, -\}$, all points in the ω-limit set of y are approached arbitrarily closely by the forward orbit of at least one of $\Phi(I_d^+)$ or $\Phi(I_d^-)$ in the asymptotic limit. Hence, if z is in the ω-limit set of $y \in R$, then z must also be in the ω-limit set of $\Phi(I_d^+)$ or of $\Phi(I_d^-)$. This concludes the proof.

The immediate consequence of this result is that there are at most two periodic orbits for bursting maps. A piecewise contractive map with two periodic orbits is shown in Figure 7(d). We can also establish a condition for such maps to yield bursting activity for all orbits.

Theorem 5.10. *If* $\omega(R) \cap I_d = \emptyset$, *then all orbits are asymptotically periodic*.

Proof. If the hypothesis is satisfied, we can define the following positive quantity:

$$\delta = \min\{d(I, I_d) : I \in \omega(R)\}. \quad (5.43)$$

We choose an arbitrary point $I \in R$. Since the orbit of I under Φ is an infinite sequence of points within a bounded interval of $\mathbb{R}^-$, ω(I) is nonempty; let $y \in \omega(I) \in \omega(R)$. We can find $\delta' < \delta$, for which $\Phi^n(B_{\delta'}(y)) \cap I_d = \emptyset$ for all $n \geq 0$. By the definition of ω-limit sets, there exists a sequence n_i such that for $I_i \doteq \Phi^{n_i}(I)$,

$$\lim_{i \to \infty} I_i = y. \quad (5.44)$$

We choose integers n_k, $n_{k'} \in \{n_i\}$ such that I_k, $I_{k'} \in B_{\delta'/2}(y)$, $k' > k$, and $|\Phi^{n_{k'}-n_k}(B_{\delta'}(y))| < \delta'/2$ (this is always possible, since Φ is contractive). Since $I_{k'} = \Phi^{n_{k'}-n_k}(I_k) \in \Phi^{n_{k'}-n_k}(B_{\delta'}(y))$, it follows that

$$\Phi^{n_{k'}-n_k}(B_{\delta'}(y)) \subset B_{\delta'}(y). \quad (5.45)$$

Since the disc $B_{\delta'}(y)$ gets mapped continuously into itself by the map $\Phi^{n_{k'}-n_k}$, there exists a unique attracting periodic orbit that attracts all $x \in B_{\delta'}(y)$, namely the orbit of y, and the orbit of I is asymptotically periodic.

5.5. Genericity of periodic behavior

In Catsigeras and Budelli (2011), we find a general treatment of injective piecewise contractions in n dimensions. We summarize an important result of their work.

Theorem 5.11 (Catsigeras and Budelli (2011)). *Injective piecewise contractive maps* C^0 *generically exhibit only asymptotically periodic behavior*.

Injectivity is necessary for this result to directly apply to bursting maps. In fact, injectivity is also used in Brémont (2006) to prove that injective piecewise contractions on the interval are generically periodic with respect to the location of a map's discontinuity points. If a refined reachable set R' exists such that $\Phi : R' \to R'$ is injective, then the conclusions of Catsigeras and Budelli (2011) hold. In particular, asymptotically periodic behavior is the only behavior that has nonzero probability of occurring in an implementation where the map is perturbed by arbitrarily small noise.

However, the arguments of Catsigeras and Budelli to prove C^0 genericity cannot be directly used to prove genericity with respect to a fixed set of parameters for our model. As pointed

out in Bruin and Deane (2009), the family of maps defined by $\Phi : [0, 1) \to [0, 1)$, $\Phi(x) = \lambda x + a \pmod 1$, for a fixed $\lambda \in (0, 1)$ and parameter $a \in [0, 1)$, is generically *aperiodic* with respect to the parameter a. It seems unlikely that a similar phenomenon occurs for parameters of our model. In the case that $\Phi' > 0$ on R, we have the following result.

Theorem 5.12. *For increasing bursting maps $\Phi : S \to S$ where S is the reachable set, $\omega(S) \cap I_d = \emptyset$ holds almost surely with respect to choice of parameters. Hence, increasing bursting maps are asymptotically periodic generically with respect to parameters of our model.*

Proof. Since Φ is increasing on S, it follows from Lemma 5.5 that we may restrict our attention to a refined reachable set R on which Φ is injective. Consider the set $E = R \backslash \Phi(R)$, referred to as the exceptional set in Bruin and Deane (2009). This set consists of points with no preimage in R. We may write

$$R = E \cup \Phi(R) = E \cup (\Phi(E) \cup \Phi^2(R)) = E \cup (\Phi(E) \cup (\Phi^2(E) \cup \Phi^3(R))),$$

and so on. Continuing this process ad infinitum we obtain

$$R = \omega(R) \cup \left(\bigcup_{i=0}^{\infty} \Phi^i(E) \right),$$

where $R = \cup_{i=0}^{\infty} \Phi^i(E)$ a.e. (almost everywhere), since $\omega(R)$ has measure zero. From injectivity, it is easy to check that these $\omega(R)$ and $\cup_{i=0}^{\infty} \Phi^i(E)$ are disjoint. As a consequence, if we can show that for an injective bursting map $I_d \in \cup_{i=0}^{\infty} \Phi^i(E)$, then we are guaranteed that $I_d \notin \omega(R)$. We claim that for increasing bursting maps, $I_d \in \cup_{i=0}^{\infty} \Phi^i(E)$ and hence $I_d \notin \omega(R)$, except for a vanishingly small subset of the parameter space. Suppose that $I_d \in (\Phi^n(E))^\circ$ for some n. Then, since I_d and $\Phi^n(E)$ both vary smoothly with respect to the parameters, there must exist a surrounding full-measure box in the parameter space defined by $p \vec{\in} \{(I_e, V_0, \Theta, I_{20}, \gamma, k_1, k_2, A_1) : I_e \in (I_{e0}, I_{e1}), \gamma \in (\gamma_0, \gamma_1), \ldots\}$ in which $I_d \in (\Phi^n(E))^\circ$ still holds.

Proposition 5.13. *Given a bursting map Φ such that $\Phi' > 0$ on a reachable set R, suppose that $I_d \in \omega(R)$ for some $A_1 = A_1'$. Given any $\delta A_1 > 0$, there exists $A_1 \in [A_1', A_1' + \delta A_1]$ such that $I_d \in \cup_{i=0}^{\infty} \Phi^i(E)$ is satisfied.*

To prove this proposition, we show that there exists an arbitrarily small perturbation of A_1 for which $I_d \in \Phi^l(E)$ for some $l > 0$. First, note that E can be written as a disjoint union of intervals: $E = \cup E_j$. Since $R = \cup_{i=0}^{\infty} \Phi^i(E)$ a.e., given any $\delta A_1 > 0$, we can always find $m > 0$ and an integer j such that the right endpoint $e_r = \sup(\Phi^m(E_j))$ satisfies

$$\delta A_1 > I_d - e_r > 0. \quad (5.46)$$

Since by assumption $I_d \notin \cup_{i=0}^{\infty} \Phi^i(E)$, the map Φ never cuts the interval E_j; that is, for each m, $\Phi^m(E_j)$ is entirely below I_d or above I_d. Since we are also taking $\Phi' > 0$, it follows that $e_r = \sup(\Phi^m(E_j)) = \Phi^m(\sup(E_j))$. We define $e_s \doteq \sup(E_j)$ such that $e_r = \Phi^m(e_s)$.

We now consider the effect of perturbing the parameter A_1 on the map Φ. From (3.2), we see that incrementing A_1 simply shifts the map Φ upwards, without changing the location of the discontinuity I_d. Increasing A_1 therefore results in an upward displacement of R as well as

$\Phi(R)$. Since $E = R\backslash\Phi(R)$, it follows that the right endpoint e_s of the set E_j will also increase to a value $e_s^{'} > e_s$ as A_1 is incremented from $A_1^{'}$ to $A_1^{'}+\delta A_1$. We now consider the perturbed map

$$\Psi(x)=\Phi(x)+\delta A_1. \quad (5.47)$$

If $I_d \in \Psi^n(E_i)$ for some $n < m$, the proposition follows immediately. Therefore, we suppose otherwise, in which case the first n iterates of E_j are not cut by Ψ. From the mean value theorem (Theorem 5.19 in Rudin, 1976), there exists a point e_1 such that we may write the second iterate of Ψ as

$$\Psi^2(e_s)=\Phi(\Phi(e_s)+\delta A_1)+\delta A_1=\Phi^2(e_s)+\delta A_1(1+\Phi'(e_1))=\Phi^2(e_s)+\delta A_1(1+\Psi'(e_1)), \quad (5.48)$$

where $\Psi(e_s) > e_1 > \Phi(e_s)$. Note that the application of the mean value theorem is appropriate unless $\Psi(e_s)$ and $\Phi(e_s)$ are on opposite sides of I_d; in that case, however, since $\Phi(E_j)$ varies continuously as A_1 is increased from $A_1^{'}$ to $A_1^{'}+\delta A_1$, there must be a point $A_1 \in [A_1^{'}, A_1^{'}+\delta A_1]$ for which $I_d \in \Phi(E_j)$ and the proposition follows. By iterating (5.48) m times we find that either $\Psi^i(e_s)$ and $\Phi^i(e_s)$ end up on opposite sides of I_d for some $1 < i < m$ and the proposition follows, or

$$\Psi^m(e_s)=\Phi^m(e_s)+\delta A_1\left(1+\sum_{j=1}^{m-1}\left(\prod_{i=j}^{m-1}\Psi'(e_i)\right)\right)=e_r+\delta A_1\left(1+\sum_{j=1}^{m-1}\left(\prod_{i=j}^{m-1}\Psi'(e_i)\right)\right), \quad (5.49)$$

where the e_i that satisfy this equation always exist (by the mean value theorem) and satisfy $\Psi^i(e_s) > e_i > \Phi^i(e_s)$. As a consequence,

$$\Psi^m(e_s^{'})>\Psi^m(e_s)>I_d>e_r, \quad (5.50)$$

from which we see that the perturbation δA_1 has pushed the interval $\Phi^m(E_i)$ across the discontinuity point I_d, which remains immobile. Thus, the continuity of $\Phi^m(E_1)$ in A_1 on $[A_1^{'}, A_1^{'}+\delta A_1]$ gives us an A_1 value for which $I_d \in \Phi^m(E_1)$. Since $\delta A_1 > 0$ was arbitrary, this result proves the proposition.

Based on the proposition, for any fixed set of parameters (I_e, V_0, Θ, I_1, I_2, γ, k_1, k_2), the set of parameters $\{\tilde{A}_1\}$ for which $I_d \in \omega(R)$ is a countable set. It follows that the set of parameters for which $I_d \notin \cup_{i=1}^{\infty}\Phi^i(E)$ has Lebesgue measure zero (see Chapter 11 in Rudin, 1976). Theorem 5.12 follows immediately.

Given this result and those in Brémont (2006) and Catsigeras and Budelli (2011), it is natural to conjecture that injective piecewise contractions are generically asymptotically periodic with respect to uniform vertical displacements. Indeed, we have not observed bursting maps for which bursting behavior does not occur, in spite of the fact that the maps generated by our model are not always injective on a refined reachable set R'. Thus, it appears that bursting maps with attracting nonperiodic orbits occupy an exceedingly small subset of the set of all bursting maps.

The above considerations suggest a simple method of partitioning R such that the iterates of points inside the same partition will be attracted to the same periodic orbit: compute the inverse orbit of I_d. Since $I_d \cap \omega(R) = \emptyset$ generically, there is a finite number of preimages $\Phi^{-i}(I_d)$ in R. By using $R \cap \{\Phi^{-i}(I_d)\}_{i=0}^{\infty}$ as boundary points, we may partition R into the union of n disjoint intervals: $R = \cup S_i$, and $S_i \cap S_j = \emptyset$ if $i \neq j$. Since the orbits of the interior of these sets never encounter the discontinuity point I_d, we are guaranteed that the interior of

the partitions S_i will be sent into each other continuously: $\Phi(S_i^\circ) \subset S_j^\circ$ for $i \neq j$. Continuing this process, for any $i \in \{1,\ldots, n\}$ there must exist integers $b > a > 0$ for which $\Phi^b(S_i^\circ) \subset \Phi^a(S_i^\circ)$. It follows that there exists a unique fixed point of the map Φ^{b-a} in some $\Phi^a(S_i^\circ) \subset S_j$ for some j. This point corresponds to a unique periodic point to which all points in S_i° are attracted. We note that such a partition $\{S_i\}$ is known in the dynamical systems literature as a *Markov partition*. Markov partitions allow us to describe the dynamics in terms of a directed graph where each vertex has a single outgoing edge. Distinct periodic orbits correspond to distinct cycles in this directed graph; the number of distinct cycles in the directed graph is equal to the number of periodic bursting solutions.

5.6. Symbolic dynamics of bursting maps

We now summarize some basic terminology from symbolic dynamics that we shall use, following conventions put forth by Lind and Marcus (1995).

Definition 5.14. *Given a point $x \in R$, we define its address $a(x)$ as* 0 *or* 1, *depending on whether x is in R_0, R_1, respectively. We define the itinerary $I(x)$ of a point $x \in R$ by the right-infinite sequence of addresses*

$$I(x)=(a(x), a(\Phi(x)), a(\Phi^2(x)), \ldots).$$

For $j \geq 0$, we define the $[i, j]$ block of an itinerary as follows:

$$I(x)_{[i,j]}=(a(\Phi^i(x)), a(\Phi^{i+1}(x)), \ldots, a(\Phi^j(x))).$$

This symbolic description of the dynamics represents a coarse graining of a point's forward trajectory. The usefulness of this approach stems from the fact that a 0 address, with $I_1 < I_d$, corresponds to a slower spike time than any iterate with a 1 address, with $I_1 > I_d$ (recall from (3.9) that larger values of I_1 result in a smaller interspike time). Therefore, the itinerary of a bursting orbit is described by a periodic succession of 1's and 0's consisting of multiple fast spikes separated by a single slow spike. For example,

$$(1, 1, 1, 0, 1, 1, 1, 0, 1, 1, 1, 0, \ldots)$$

corresponds to a periodic pattern of bursts of three spikes, also known as triplets. In the case that Φ is piecewise injective on R, the dynamics are dramatically simplified and are suggestive of bursting. As discussed previously, many of the bursting maps observed in our model satisfy the piecewise injective property on the reachable set R in addition to the piecewise contractive property.

Theorem 5.15. *Suppose a bursting map Φ is piecewise injective on R. Given $i \in \{0, 1\}$ and $x_0 \in R_i$, we define $M = \min\{m : \Phi^m(x_0) \in R_{1-i}\}$. Then, for any $m > M$, there exists $j \in \{0, 1\}$ such that if $\Phi^m(x) \in R_j$, then $\Phi^{m+1}(x) \in R_{1-j}$.*

Proof. The theorem states that after M iterates, the itinerary of x cannot contain both consecutive 1's (fast spikes) and consecutive 0's (slow spikes).

- *Case* I: $\Phi'(x) < 0$ on R_i for some i.

  If $\Phi'(x) < 0$ on R_i, then for all $x \in R_i$, $\Phi(x) \in R_{1-i}$, satisfying the theorem.

- *Case* II: $\Phi'(x) > 0$ on R_0 and R_1.

We proceed by contradiction. Suppose there exist m_1, $m_2 > M$ such that

$$\begin{aligned} a(\Phi^{m_1}(x))=0, \quad a(\Phi^{m_1+1}(x))=0, \\ a(\Phi^{m_2}(x))=1, \quad a(\Phi^{m_2+1}(x))=1. \end{aligned} \tag{5.51}$$

By definition, Φ is increasing on R_0 and on R_1. In addition, since m_1, $m_2 > M$, $\Phi^{m1}(x)$ has a preimage in R_1, and $\Phi^{m2}(x)$ has a preimage in R_0. Since $R_1 \geq I_d \geq R_0$, it follows that

$$\Phi(I_d^+)<\Phi^{m_1}(x)<\Phi^{m_1+1}(x)<I_d,\ I_d<\Phi^{m_2+1}(x)<\Phi^{m_2}(x)<\Phi(I_d^-). \tag{5.52}$$

From the positivity of $\Phi'(x)$ on R_0, R_1, we may apply Φ to the preceding inequalities, obtaining

$$\Phi^2(I_d^+)<\Phi^{m_1+1}(x)<I_d,\ I_d<\Phi^{m_2+1}(x)<\Phi^2(I_d^-). \tag{5.53}$$

From the contractive property of Φ,

$$d(\Phi(I_d^+), I_d)>d(\Phi^2(I_d^+), \Phi(I_d^-)),\ d(I_d, \Phi(I_d^-))>d(\Phi(I_d^+), \Phi^2(I_d^-)). \tag{5.54}$$

Inequalities (5.52) and (5.53) imply that

$$\Phi(I_d^-)>I_d>\Phi^2(I_d^+),\ \Phi^2(I_d^-)>I_d>\Phi(I_d^+) \tag{5.55}$$

such that

$$d(\Phi^2(I_d^+), \Phi(I_d^-))>d(I_d, \Phi(I_d^-)),\ d(\Phi(I_d^+), \Phi^2(I_d^-))>d(\Phi(I_d^+), I_d). \tag{5.56}$$

Combining (5.54) and (5.56) gives us the required contradictions.

The following similar result about periodic orbits holds for arbitrary bursting maps and does not suppose injectivity.

Theorem 5.16. *Given a bursting map Φ with periodic orbit $\{x_0, x_1, x_2, \ldots, x_0, \ldots\}$, the following two itinerary blocks are mutually incompatible*:

$$I(x_0)_{[n,n+1]}=(0,0),\ I(x_0)_{[m,m+1]}=(1,1) \tag{5.57}$$

for any n,m > 0. For example, if there exists an n such that the first condition holds, the second is false for all m > 0.

Proof. We show this result by contradiction. Assume there indeed exist $y_1 \in R_0$, $z_1 \in R_1$ on which $\Phi(y_1) \in R_0$, $\Phi(z_1) \in R_1$. Since the periodic orbit is a finite set for which the map Φ is bijective, we may apply the inverse map Φ^{-1} to this set without difficulty even in cases where Φ is not injective on R. Define

$$x_{min}=\min(\{x_i\}), x_{max}=\max(\{x_i\}),\ y_0=\Phi^{-1}(x_{max}) \in R_0, z_0=\Phi^{-1}(x_{min}) \in R_1. \tag{5.58}$$

The memberships of y_0, z_0 to the sets R_0, R_1 follow from the definition of a bursting map: for any $a_0 \in R_0$ and $a_1 \in R_1$, $\Phi(a_0) > a_0$ and $\Phi(a_1) < a_1$. Then,

$$d(I_d, x_{min})>d(y_0, y_1)>d(\Phi(y_0), \Phi(y_1))>d(I_d, x_{max}), \tag{5.59}$$

where we have used the fact that $\Phi(y_0) = x_{max}$. Similarly,

$$d(I_d, x_{max}) > d(z_0, z_1) > d(\Phi(z_0), \Phi(z_1)) > d(I_d, x_{min}), \quad (5.60)$$

which gives us the required contradiction.

If $\Phi(R_0) \subset R_1$, there cannot be successive slow spikes, and if $\Phi(R_1) \subset R_0$, there cannot be successive fast spikes. If the map's derivative is sufficiently small on R_0, we are guaranteed that $\Phi(R_0) \subset R_1$. We now make this statement precise.

Proposition 5.17. *Given a bursting map* Φ, *define* $\varepsilon = \sup\{\varepsilon_1 : \Phi(I) - I > \varepsilon_1$ *for all* $I \in R_0\}$, *and define* $r_{min} = \min(R_0)$. *If*

$$\Phi'(I) < \frac{\varepsilon}{I_d - r_{min}} \forall I \in R_0, \quad (5.61)$$

then $\Phi(R_0) \subset R_1$, *and there are no consecutive slow spikes once the iterates are inside the reachable set R.*

Proof. Suppose, on the contrary, that $\Phi(R_0) \cap R_0 \neq \emptyset$. Then, there exists $r_0 \in R_0$ such that $\Phi(r_0) = r_1 < I_d$. We also have $\Phi(r_1) > r_1 + \varepsilon$. From the mean value theorem, there exists $y \in R_0$ such that

$$\Phi'(y)(r_1 - r_0) = \Phi(r_1) - \Phi(r_0) > \varepsilon. \quad (5.62)$$

By the definition of the reachable set R (Definition 5.4), we have $R_0 = [r_{min}, I_d)$. Hence,

$$\Phi'(y) > \frac{\varepsilon}{r_1 - r_0} > \frac{\varepsilon}{I_d - r_{min}}, \quad (5.63)$$

which contradicts the hypothesis of the lemma.

This proposition shows that if Φ' is sufficiently small at every point in R_0 (or is negative), we will not observe periodic bursting orbits in which multiple slow spikes are separated by single fast spikes, such as

$$(0, 0, 0, 1, 0, 0, 0, 1, 0, 0, 0, 1, \ldots).$$

In our model, $|\Phi'|$ is often small on R_0, and hence $\Phi(R_0) \subset R_1$ is commonly observed. This is seen in Figure 4(b).

6. Co-existence of solutions and transitions between them

In the previous two sections, we have focused separately on the dynamics of tonic spiking and bursting in model (2.1)–(2.2). We conclude our analysis by considering how transitions between solution regimes, including scenarios where solution types co-exist, occur as parameters are varied.

6.1. Quiescent and phasic solutions

We have already seen that if condition (2.7) holds, then all initial conditions lead to spikes, so we avoid that condition for now.

Proposition 6.1. *If* (2.7) *is false, then for any initial value* I_{20} *(or, equivalently, any value of* A_2*), there exists some* $I_q \in \mathbb{R}^-$ *such that for all initial values* $I_{10} < I_q$, *the neuron does not spike, and for all initial values* $I_{10} \geq I_q$, *the neuron spikes.*

Proof. From the model solutions (see (2.3)), we have

$$V(t)<V_0+\frac{I_e}{\gamma}+\frac{I_{10}}{\gamma-k_1}(\exp(-k_1t)-\exp(-\gamma t))+\frac{I_{20}}{\gamma-k_2}(\exp(-k_2t)-\exp(-\gamma t)). \quad (6.1)$$

We rewrite the above inequality as

$$V(t)<V_0+\frac{I_e}{\gamma}+I_{10}g(t)+I_{20}h(t), \quad (6.2)$$

where $g(t)$, $h(t) > 0$ for all $t > 0$. If the neuron does not spike for $I_{10} = 0$, then we choose $I_q = 0$ and the proposition follows. Assume instead that the neuron does spike for $I_{10} = 0$. In this case, for $I_{10} = 0$, there exist times t_a, t_b such that $\Theta \le V(t)$ if and only if $t \in [t_a, t_b]$, since the voltage in this case is a sum of two exponentials. In this time interval, the inequality

$$\Theta - V_0 - \frac{I_e}{\gamma}<I_{20}h(t) \quad (6.3)$$

follows from (6.2). We now define

$$I_q^*=\frac{\Theta - V_0 - \frac{I_e}{\gamma} - I_{20}\max_{t_a<t<t_b}h(t)}{\min_{t_a<t<t_b}g(t)}<0. \quad (6.4)$$

It is readily checked that for any $I_{10}<I_q^*$, we have $V(t) < \Theta$ for any $t > 0$, and the neuron does not spike. Of course, since the voltage time course increases monotonically with I_{10}, there exists some $I_q \ge I_q^*$ that satisfies the criterion of the proposition.

6.2. Onset of tonic spiking

In spite of Proposition 6.1, the failure of condition (2.7) does not rule out sustained spiking entirely if A_2 is sufficiently large.

Proposition 6.2. *Suppose* (2.7) *is false and* A_2 *is sufficiently large such that the neuron spikes for some* $I_{10} = I_{1s} < 0$. *There exists a value of the reset parameter* $A_1=A_1^*<0$ *for which tonic spiking co-exists with quiescent solutions, as selected by initial conditions. Similarly, there exists a value of the reset parameter* $A_1=A_1^{**}<0$ *for which phasic solutions co-exist with quiescent solutions, as selected by initial conditions.*

Proof. To prove the first part of the proposition, consider that the trajectory associated with $I_{10} = I_{1s}$ yields a spike at a time $t = t_s$. Choose $A_1^*=I_{1s}(1 - e^{-k_1t_s})$. From the map definition (3.2), if we set $A_1=A_1^*$, we have $\Phi(I_{1s}) = I_{1s}$, which is the fixed point equation corresponding to tonic spiking solutions. On the other hand, from Proposition 6.1, there exists some I_q such that trajectories with $I_{10} < I_q$ cannot reach threshold, and thus co-existence between tonic spiking and quiescence is achieved. This concludes the first part of the proposition.

To prove the second part of the proposition, choose a value of the reset parameter $A_1=A_1^{**}$ that satisfies

$$A_1^{**}<\min_{I_{10}>I_q}\{I_{10}(1-\exp(-k_1t(I_{10})))\}<0, \quad (6.5)$$

where we write $t(I_{10})$ to emphasize that the spike time t itself depends on the initial value of the I_1 current. It follows that

$$\max_{I_{10}>I_q}\{A_1+I_{10}(\exp(-k_1t(I_{10})-1))\}=\max_{I_{10}>I_d}\{\Phi(I_{10})-I_{10}\}<0. \quad (6.6)$$

Thus, the fixed point equation $\Phi(I_{10}) = I_{10}$ is never satisfied. Since the map is decreasing, if we set $I_{10} = 0$, there exists a finite number m of spikes, with $\Phi^k(0) \geq I_q$ for all $k < m$ and $\Phi^m(0) < I_q$, after which the neuron will not spike, as established in Proposition 6.1. This situation corresponds to a phasic spiking solution. On the other hand, if we choose $I_{10} < I_q$, the solution will be quiescent. This concludes the proof of the second part of the proposition.

The above proof illustrates that for appropriate choices of A_2, very negative choices of A_1 lead to termination of spiking after finitely many spikes, while a smaller magnitude choice of A_1 can yield tonic spiking. That is, we can obtain a bifurcation from the absence of sustained spiking to the appearance of a tonic spiking fixed point by increasing the parameter A_1, which shifts the map vertically (see (3.2)). This bifurcation is illustrated in Figures 8(a)–8(d).

6.3. Onset of bursting

From Proposition 5.1, condition (2.7) must hold for bursting to occur. Hence, to switch from quiescent or phasic spiking to bursting, parameters must be varied that cause (2.7) to hold. Once (2.7) holds, however, all initial conditions lead to sustained spiking. We thus observe that we have two possible routes away from parameter regimes that lack sustained spiking, for which the return map is defined only on a finite interval of I_1 values. In the case illustrated in Figures 8(a)–8(d), as a parameter is varied, a fixed point comes into existence before condition (2.7) becomes satisfied, yielding co-existence of quiescent solutions with tonic or phasic solutions. Alternatively, as a parameter is varied, condition (2.7) may become true before a fixed point exists, in which case the return map becomes defined for all $I_1 \leq 0$ and, at least for parameter values near this event, exhibits a discontinuity at some value $I_1 = I_d < 0$.

Due to the form of condition (2.7), a natural parameter to vary to attain the transition from phasic spiking to bursting is I_e. Figures 9(a)–9(d) show an example of this transition as I_e is increased, with other parameters fixed as in the last row in Table 1.

6.4. From bursting to tonic spiking

Increasing the input current I_e causes the return map Φ to decrease. This property follows from the map definition

$$\Phi(I_1)=I_1x^{k_1}+A_1 \quad (6.7)$$

and the fact that increasing I_e always makes the neuron spike sooner: $\frac{dx}{dI_e}>0$. Furthermore, increases in I_e yield decreases in the I_1 value at the discontinuity, I_d, of Φ. To see this result, define the function $f: \mathbf{R}^3 \to \mathbf{R}^2$ by

$$f(x,I_e,I_1)=[D(x,I_e,I_1),D'(x,I_e,I_1)]^\top, \quad (6.8)$$

where $D(x, I_e, I_1)$ is given in (2.4) and $D'(x,I_e,I_1)=\frac{\partial D(x,I_e,I_1)}{\partial x}$. For a given I_e, the value of I_d is determined by the equation $f(x, I_e, I_1) = \mathbf{0}$ at $I_1 = I_d$.

Proposition 6.3. *The discontinuity point* (x, I_d) *of the map* Φ *depends smoothly on the parameter* I_e *whenever the Jacobian matrix*

$$Df = \begin{bmatrix} \frac{\partial D(x,I_e,I_d)}{\partial x} & \frac{\partial D(x,I_e,I_d)}{\partial I_1} \\ \frac{\partial D'(x,I_e,I_d)}{\partial x} & \frac{\partial D'(x,I_e,I_d)}{\partial I_1} \end{bmatrix} \quad (6.9)$$

is invertible. In addition,

$$\frac{dI_d}{dI_e} < 0. \quad (6.10)$$

Proof. The smoothness of the variation of x, I_d with respect to I_e follows directly from the generalized implicit function theorem. To show $dI_d/dI_e < 0$, we consider perturbations of x, I_e, I_1 on the manifold defined by $D(x, I_e, I_1) = \mathbf{0}$. To first order, these perturbations satisfy

$$\Delta x \left(\frac{\partial D(x, I_e, I_1)}{\partial x} \right) + \Delta I_1 \left(\frac{\partial D(x, I_e, I_1)}{\partial I_1} \right) + \Delta I_e \left(\frac{\partial D(x, I_e, I_1)}{\partial I_e} \right) = 0. \quad (6.11)$$

However, note that at any discontinuity associated with bursting, $\partial D(x, I_e, I_1)/\partial x = 0$, $\partial D(x, I_e, I_1)/\partial I_e > 0$, and $\partial D(x, I_e, I_1)/\partial I_1 > 0$. It follows that $\Delta I_1/\Delta I_e < 0$, thus completing the proof.

As I_e is increased, we therefore have the lower segment of Φ (with $0 \geq I_1 > I_d$) moving to more negative values and extending over a larger interval of I_1. A transition to tonic spiking will occur if a transition occurs in which this part of the map collides with the identity line, resulting in the creation of a new fixed point. In the literature, this is known as a *border collision bifurcation* (Helena and James, 1995; Jain and Banerjee, 2003). The map-decreasing effect of increasing I_e opposes the creation of a fixed point, while the discontinuity-shifting effect of increasing I_e promotes it. Figures 10(a)–10(d) illustrate a case in which the latter effect is dominant and increases in I_e cause a transition from bursting to tonic spiking.

7. Discussion

In this paper, we have studied the contractive dynamics that typically arise in a simple generalized integrate-and-fire model. The model, a special case of the model introduced by Mihalas and Niebur (2009), consists of a linear, diagonalizable set of differential equations combined with an update rule that is applied whenever the membrane voltage crosses the threshold. In our analysis, we significantly advance our understanding of the more general model described in Mihalas and Niebur (2009) by deriving a discrete return map that accurately describes the model's sustained activity patterns, tonic spiking and bursting. We establish certain general properties of this map, discuss conditions for tonic spiking, bursting, and asymptotic periodicity of solutions, and consider transitions between solution types.

Our results are likely to be of practical interest to researchers, since our model produces a variety of spiking behaviors in a manner that is naturally conducive to computational implementation using efficient event-driven algorithms (Mihalas et al., 2011) and even for implementations in VLSI hardware (Folowosele et al., 2009; van Schaik et al., 2010). An important objective of neural network simulations is to study the link between the properties of single neurons and network dynamics. As such, the ability to design efficiently implemented model neurons that provably possess certain properties, such as bursting and tonic firing, is of significant utility.

Local contractivity of the return map played a key role in our analysis. We used analytical formulas for model solutions to derive an exact closed form expression, (3.5), for the derivative of the return map at every point. This expression allowed us to find mild conditions on the parameters for local contractivity without the need for sophisticated estimates, in contrast to the methodology developed in Foxall et al. (2012) to find sufficient conditions for tonic spiking in a model with nonlinear dynamics.

Our results include some general findings on how piecewise contractive maps can capture bursting behavior. We demonstrate that the piecewise contractive property not only admits at most two periodic orbits but also enforces a strong constraint on the symbolic dynamics that may be observed. If the map is injective, then after the orbit crosses the discontinuity point I_d once, all orbits must consist of one or more fast (slow) spikes separated by single slow (fast) spikes. If the map is not injective, its orbits are attracted to periodic orbits with a similar property, namely that they cannot feature repeated slow spikes followed by repeated fast spikes. In particular, if the map has a sufficiently small or negative derivative on the part of its domain corresponding to slow spikes, then we observe the typical bursting phenomenon of multiple fast spikes separated by single slow spikes. Thus, piecewise contractions provide a simple and elegant abstraction for bursting in biological neurons.

Contraction approaches have been used successfully in the study of continuous nonlinear systems (see Lohmiller and Slotine, 1998). The power of the contraction approach stems from the fact that it employs a simpler notion of stability. Instead of viewing stability from the global point of view of convergence to nominal trajectories that in practice may be difficult to compute, the contraction approach views stability from a local point of view: temporary disturbances are “forgotten,” and nearby trajectories converge to the same trajectory. The contractive notion of stability appears especially well suited to modeling neural systems, as contractive systems are inherently forgiving of sufficiently small stochastic effects and can compute reliably in their presence. Piecewise contraction analysis is the natural extension of contraction analysis to dynamical systems that compute symbolically, as neural systems appear to do. It has been shown that under certain conditions, spiking neural networks are piecewise contractive (Catsigeras and Guiraud, to appear; Cessac, 2008). A limitation of these works is that their predictions are not experimentally verifiable. By showing that bursting, an observed behavior, can be modeled effectively in the piecewise contraction framework, we lend credibility to the piecewise contraction approach as a model of neural system dynamics.

Bursting dynamics also arise in other reset-based models. Two prominent examples are the integrate-and-burst model of Coombes, Owen, and Smith (2001) and the Izhikevich model of Izhikevich (2004). In the former case, an additional nonlinear current and associated threshold are appended to the standard leaky integrate-and-fire model to generate bursting, while the latter features a quadratic voltage equation, such that the bursting mechanisms in both models are more complicated than the one we consider. Map-based representations of bursting have been directly proposed, but these are two-dimensional (Rulkov, 2002; Shilnikov and Rulkov, 2003) or have been derived from nonlinear conductance-based models (Medvedev, 2005) (see Ibarz, Casado, and Sanjuán, 2011 for a review of map models in neuroscience). In the latter case, the onset of bursting can be associated with the loss of stability of a fixed point, and resulting chaotic dynamics have been analyzed by Medvedev (2006). As in Izhikevich (2004), the variable in our model that undergoes an additive reset (reset to a nonconstant value) has an adaptive effect on voltage dynamics, hindering the approach to threshold. In other works, maps have been derived from oscillators coupled with synaptic inhibition, which also holds back spiking (Medvedev and Cisternas, 2004; Zhang, Bose, and Nadim, 2009). While this mechanism can lead to nontrivial oscillations and phase locking, it differs from what we consider in that the timing

with which inhibitory signals arrive at one oscillator is determined by the state of the other oscillator, rather than by the impacted oscillator itself.

A limitation of our work is the lack of a sufficient analytical condition on the parameters to ensure the piecewise contractive property of the return map. We leave the task of finding such a condition for further research. For practical purposes, it is a simple matter to check the property computationally by using (3.5), as was done in section 3.2. The more general problem of identifying classes of impulsive hybrid systems whose return maps have the piecewise contractive property is another open avenue for research. The simplest way to induce piecewise contractive maps from system dynamics is by switching between a finite number of globally contractive system dynamics based on the previous post-reset value of an adaptation variable (in our case, I_1). For example, given state vector $\mathbf{x} = [x_1,\ldots, x_m]^\top$, adaptation variable x_1, whose previous initial value we denote by x_{10}, a set of globally contractive system dynamics $\{\varphi_i\}_{i=1}^n$, and a corresponding partition $\cup_{i=1}^n S_i$ of the domain of x_1, the following dynamics are piecewise contractive:

$$k{=}\zeta(x_{10}) \in \{1,\ldots,n\},\ \dot{\mathbf{x}}{=}\varphi_k(\mathbf{x}),\ \mathbf{x} \leftarrow \Omega(\mathbf{x}) \text{if} \mathbf{x} \in D, \quad (7.1)$$

where ζ is the discrete-valued selection function which chooses k depending on the previous value of x_{10}, D is the forbidden set, and Ω is the reset function that resets all x_i to a constant value except for the adaptation variable x_1 (which is incremented in our case). Of course, the global contractivity of the set of system dynamics $\{\varphi_i\}_{i=1}^n$ itself depends on the shape of the forbidden set D as well as the reset function Ω. In the analysis of spiking neural models, the forbidden set is defined by $V(t) \geq \Theta(t)$. This formulation is closely aligned with the classical definition of a hybrid system, in which the state of the system is described by the values of the continuous variables as well as the discrete-valued *control mode*.

The goal of single neuron modeling should not only be to replicate observed behaviors with biologically plausible models but also to derive the most parsimonious algorithmic rules that result in such behaviors. Neurons have been observed to fire in repetitive patterns when a constant input current is given. In this paper, we have shown that the locally contractive property of the adaptation variable in our neuron model is sufficient to induce asymptotically stable tonic spiking and bursting. Local contractions can also accommodate other behaviors that we have discussed as well, such as phasic spiking and the co-existence of spiking patterns. The results of our paper are of a general nature and may be applied to the analysis of other spiking models. It is our hope that our work contributes a useful framework for understanding nonchaotic spiking dynamics.

REFERENCES

Brémont J. Dynamics of injective quasi-contractions. Ergodic Theory Dynam. Systems. 2006; 26:19–44.

Brette R. Exact simulation of integrate-and-fire models with exponential currents. Neural Comput. 2007; 19:2604–2609. [PubMed: 17716004]

Bruin H, Deane J. Piecewise contractions are asymptotically periodic. Proc. Amer. Math. Soc. 2009; 137:1389–1395.

Brunel N, van Rossum M. Lapicque's 1907 paper: From frogs to integrate-and-fire. Biol. Cybernet. 2007; 97:337–339.

Catsigeras E, Budelli R. Topological dynamics of generic piecewise continuous contractive maps in n dimensions. Int. J. Pure Appl. Math. 2011; 68:61–83.

Catsigeras E, Guiraud P. Integrate and fire neural networks, piecewise contractive maps and limit cycles. J. Math. Biol. 65 (to appear).

Cessac B. A discrete time neural network model with spiking neurons. J. Math. Biol. 2008; 56:311–345. [PubMed: 17874106]

Coombes S, Owen MR, Smith G. Mode locking in a periodically forced integrate-and-fire-orburst neuron model. Phys. Rev. E. 2001; (3):64. 041914.

Donde V, Hiskens IA. Grazing bifurcations in periodic hybrid systems. Proceedings of the 2004 IEEE International Symposium on Circuits and Systems (ISCAS'04). 2004; Vol. 4 IV–697.

Folowosele, F.; Harrison, A.; Cassidy, A.; Andreou, AG.; Etienne-Cummings, R.; Mihalas, S.; Niebur, E.; Hamilton, TJ. A switched-capacitor implementation of the generalized linear integrate-and-fire neuron; Proceedings of the IEEE International Symposium on Circuits and Systems (ISCAS, Taiwan); 2009. p. 2149-2152.

Foxall E, Edwards R, Ibrahim S, van den Driessche P. A contraction argument for two-dimensional spiking neuron models. SIAM J. Appl. Dyn. Syst. 2012; 11:540–566.

Gambaudo J, Tresser C. On the dynamics of quasi-contractions. Bol. Soc. Brasil. Mat. 1988; 19:61–114.

Haddad W, Chellaboina V, Kablar N. Non-linear impulsive dynamical systems. Part I: Stability and dissipativity. Internat. J. Control. 2001; 74:1631–1658.

Helena EN, James AY. Border-collision bifurcations for piecewise smooth one-dimensional maps. Internat. J. Bifur. Chaos Appl. Sci. Engrg. 1995; 5:189–207.

Henzinger, T. The theory of hybrid automata; Proceedings of the Eleventh Annual IEEE Symposium on Logic in Computer Science (LICS'96); 1996. p. 278-292.

Hogan S, Higham L, Griffin T. Dynamics of a piecewise linear map with a gap. Proc. R. Soc. Lond. Ser. A Math. Phys. Eng. Sci. 2007; 463:49–65.

Ibarz B, Casado J, Sanjuán M. Map-based models in neuronal dynamics. Phys. Rep. 2011; 501:1–74.

Izhikevich E. Which model to use for cortical spiking neurons? IEEE Trans. Neural Networks. 2004; 15:1063–1070.

Izhikevich E, Hoppensteadt F. Classification of bursting mappings. Internat. J. Bifur. Chaos Appl. Sci. Eng. 2004; 14:3847–3854.

Jain P, Banerjee S. Border-collision bifurcations in one-dimensional discontinuous maps. Internat. J. Bifur. Chaos Appl. Sci. Engrg. 2003; 13:3341–3351.

Knight B. Dynamics of encoding in a population of neurons. J. Gen. Physiol. 1972; 59:734–766. [PubMed: 5025748]

Kruglikov B, Rypdal M. A piece-wise affine contracting map with positive entropy. Discrete Contin. Dyn. Syst. 2006; 16:393–394.

Lajoie G, Shea-Brown E. Shared inputs, entrainment, and desynchrony in elliptic bursters: From slow passage to discontinuous circle maps. SIAM J. Appl. Dyn. Syst. 2011; 10:1232–1271.

Lind, D.; Marcus, B. An Introduction to Symbolic Dynamics and Coding. Cambridge, UK: Cambridge University Press; 1995.

Lohmiller W, Slotine J. On contraction analysis for non-linear systems. Automatica J. IFAC. 1998; 34:683–696.

Manica E, Medvedev GS, Rubin JE. First return maps for the dynamics of synaptically coupled conditional bursters. Biol. Cybernet. 2010; 103:87–104.

Medvedev G. Reduction of a model of an excitable cell to a one-dimensional map. Phys. D. 2005; 202:37–59.

Medvedev GS. Transition to bursting via deterministic chaos. Phys. Rev. Lett. 2006; 97:48102.

Medvedev GS, Cisternas JE. Multimodal regimes in a compartmental model of the dopamine neuron. Phys. D. 2004; 194:333–356.

Mihalas, S.; Dong, Y.; von der Heydt, R.; Niebur, E. Event-related simulation of neural processing in complex visual scenes; Proceedings of the 45th Annual IEEE Conference on Information Sciences and Systems (IEEE-CISS-2011); Baltimore, MD. 2011. p. 1-6.

Mihalas S, Niebur E. A generalized linear integrate-and-fire neural model produces diverse spiking behaviors. Neural Comput. 2009; 21:704–718. [PubMed: 18928368]

Nagumo J, Sato S. On a response characteristic of a mathematical neuron model. Biol. Cybernet. 1972; 10:155–164.

Rudin, W. Principles of Mathematical Analysis. Vol. Vol. 3. New York: McGraw-Hill; 1976.

Rulkov N. Modeling of spiking-bursting neural behavior using two-dimensional map. Phys. Rev. E. 2002; (3):65. 041922.

Sharkovskiĭ A. Coexistence of cycles of a continuous map of the line into itself. Internat. J. Bifur. Chaos Appl. Sci. Engrg. 1995; 5:1263–1273.

Shilnikov A, Rulkov N. Origin of chaos in a two-dimensional map modeling spiking-bursting neural activity. Internat. J. Bifur. Chaos Appl. Sci. Engrg. 2003; 13:3325–3340.

Touboul J, Brette R. Spiking dynamics of bidimensional integrate-and-fire neurons. SIAM J. Appl. Dyn. Syst. 2009; 8:1462–1506.

van Schaik, A.; Jin, C.; McEwan, A.; Hamilton, T.; Mihalas, S.; Niebur, E. A log-domain implementation of the Mihalas-Niebur neuron model; Proceedings of the 2010 IEEE International Symposium on Circuits and Systems (ISCAS); 2010. p. 4249-4252.

Zhang Y, Bose A, Nadim F. The influence of the A-current on the dynamics of an oscillator-follower inhibitory network. SIAM J. Appl. Dyn. Syst. 2009; 8:1564–1590. [PubMed: 20664815]

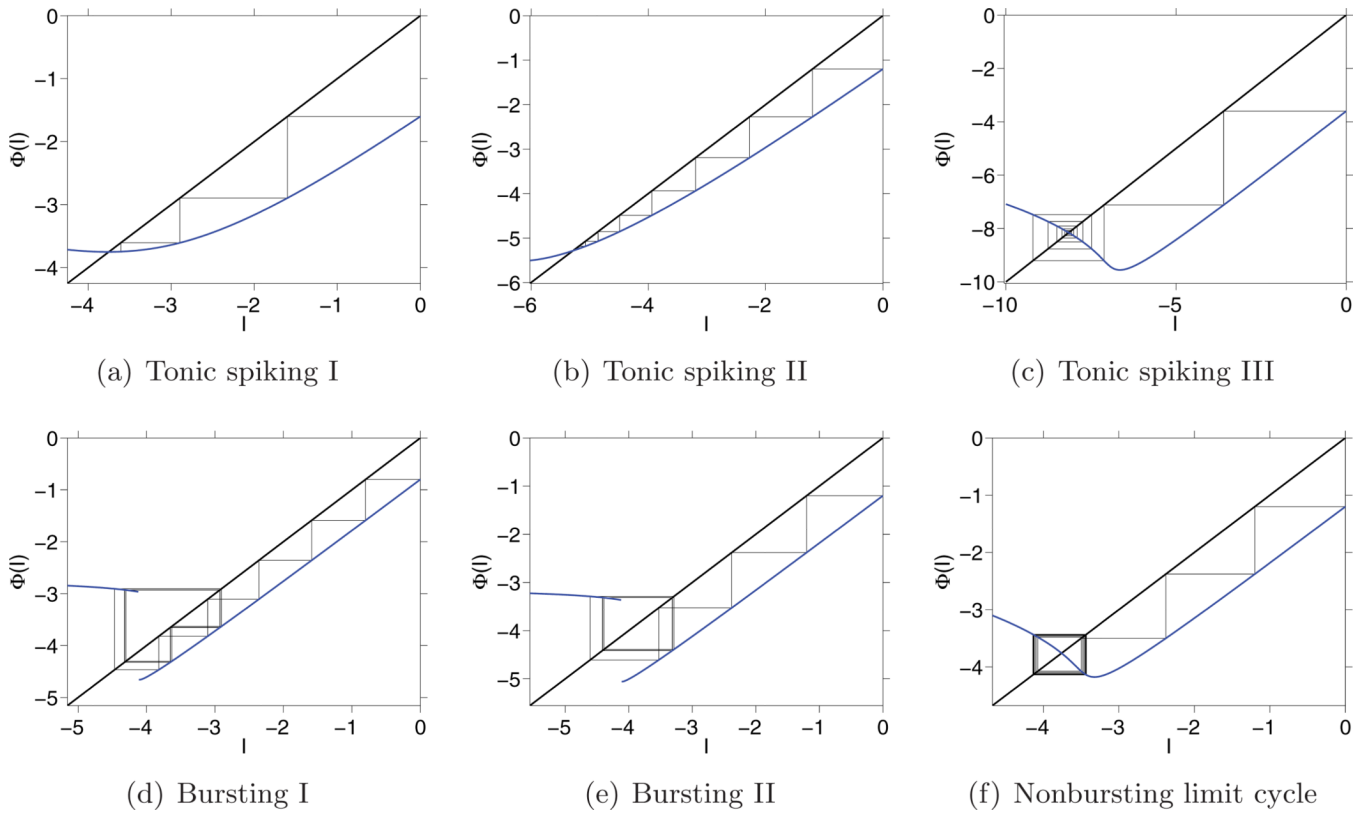

Figure 1.

Examples of return maps for various spiking scenarios. The blue curve is the function Φ(I), the black diagonal line is the identity, and the black line with horizontal and vertical segments connects system states between spikes. By iterating the map graphically—a procedure known as cobwebbing—we gain insight into its asymptotic dynamics. Comparing (a) and (b), we see that the orbits of maps with smaller derivatives converge in fewer iterations to the fixed point than of maps with larger derivatives. All maps except for (f) satisfy the piecewise contractive property. The maps were generated from the model using parameters listed in Table 1. As will be seen in (3.9), larger iterates of I result in a shorter interspike interval (faster spike time).

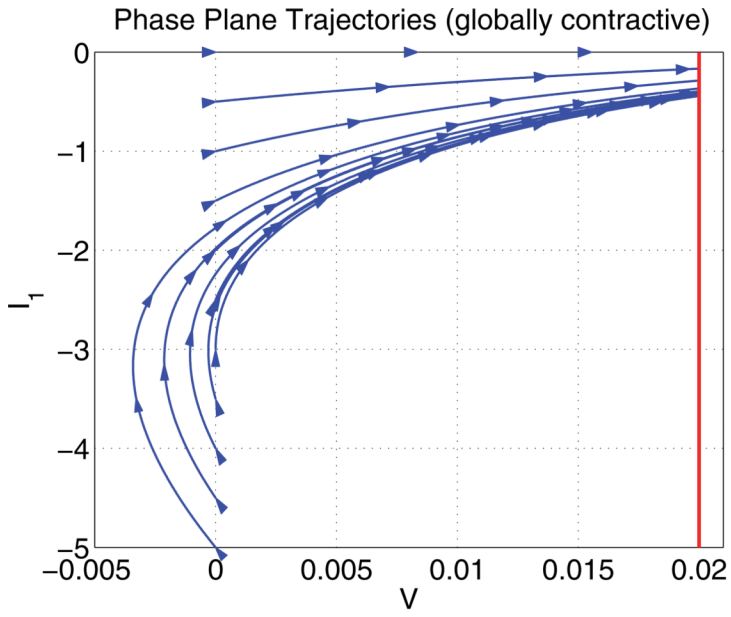

(a) Globally contractive trajectories

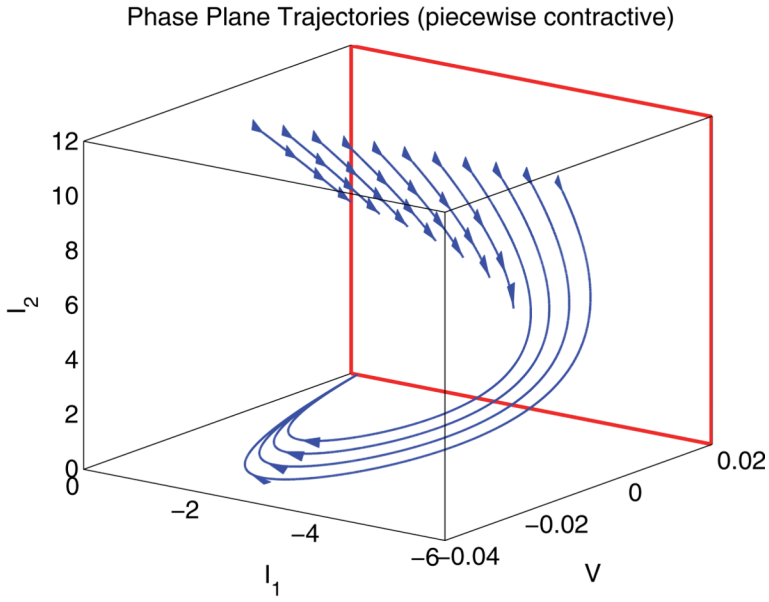

(b) Piecewise contractive trajectories

Figure 2.

Trajectories of contractive and piecewise contractive maps. Collections of trajectories were simulated, starting from $V = V_0 = 0$ and equally spaced I_{10} values and continuing until $V = \Theta = 0.02$ was reached. The blue lines with arrows represent trajectories, and the red lines are used to illustrate the spiking surface $V = \Theta$. (a) Phase plane trajectories for a globally contractive case, resulting in tonic spiking. Additional parameter values used are $I_{20} = 0$, $k_1 = 120$, $\gamma = 50$, $I_e = 3$. (b) Phase space trajectories for a piecewise contractive case, resulting in bursting. A three-dimensional phase space was used, because here $I_2 \neq 0$. A set of trajectories with I_{10} values near 0 hits $V = \Theta$ quickly, while another set makes a longer

excursion before doing so. Additional parameter values used are $I_{20} = 10$, $k_1 = 20$, $k_2 = 200$, $\gamma = 40$, $I_e = 1$.

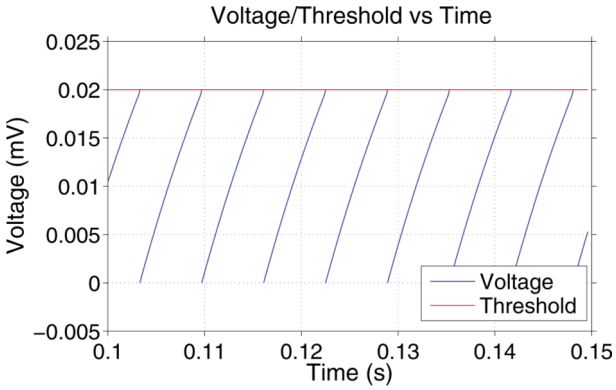

(a) Voltage time course

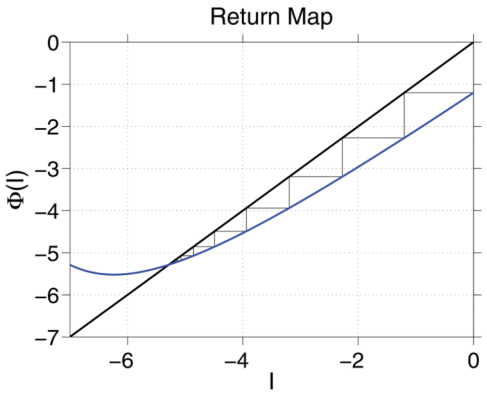

(b) Return Map

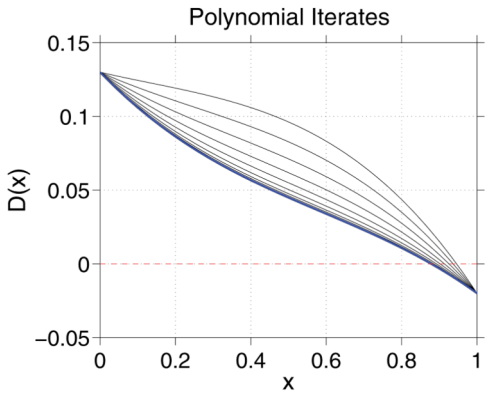

(c) Iterates of $D(x)$

Figure 3.

Visualization of a tonically firing neuron. See Table 1 for parameters used. (a) Converged dynamics corresponding to the fixed point of Φ. (b) The Poincaré return map is globally contractive. (c) Graph of D(x) for the values of I_{10} that occurred in the simulation shown in (a). The blue line corresponds to the iterate of D(x) computed at the end of simulation shown in (a).

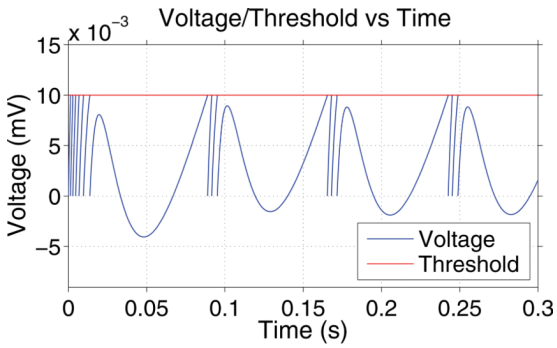

(a) Voltage time course

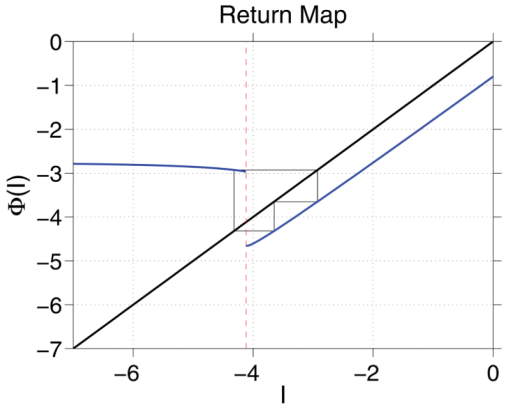

(b) Return map

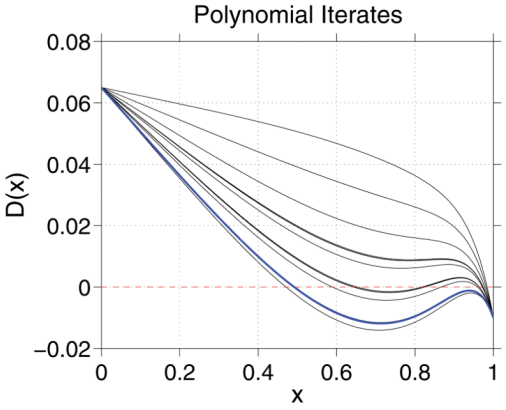

(c) Iterates of $D(x)$

Figure 4.

Visualization of a bursting model neuron. See Table 1 for the parameters used. (a) The voltage time course shows that voltage reaches threshold several times within each burst. Notice the initial transient burst, after which Φ, as shown in (b), is confined to the reachable set. (b) The return map Φ(I) is piecewise contractive. The right side of the discontinuity corresponds to fast spikes, and the left side corresponds to slow spikes. (c) D(x) for the post-reset values of I_1 that occurred in the simulation shown in (a). D(x) can gain or lose a root in (0,1) as I_1 evolves. The blue line corresponds to the iterate of D(x) computed at the end of the simulation shown in (a).

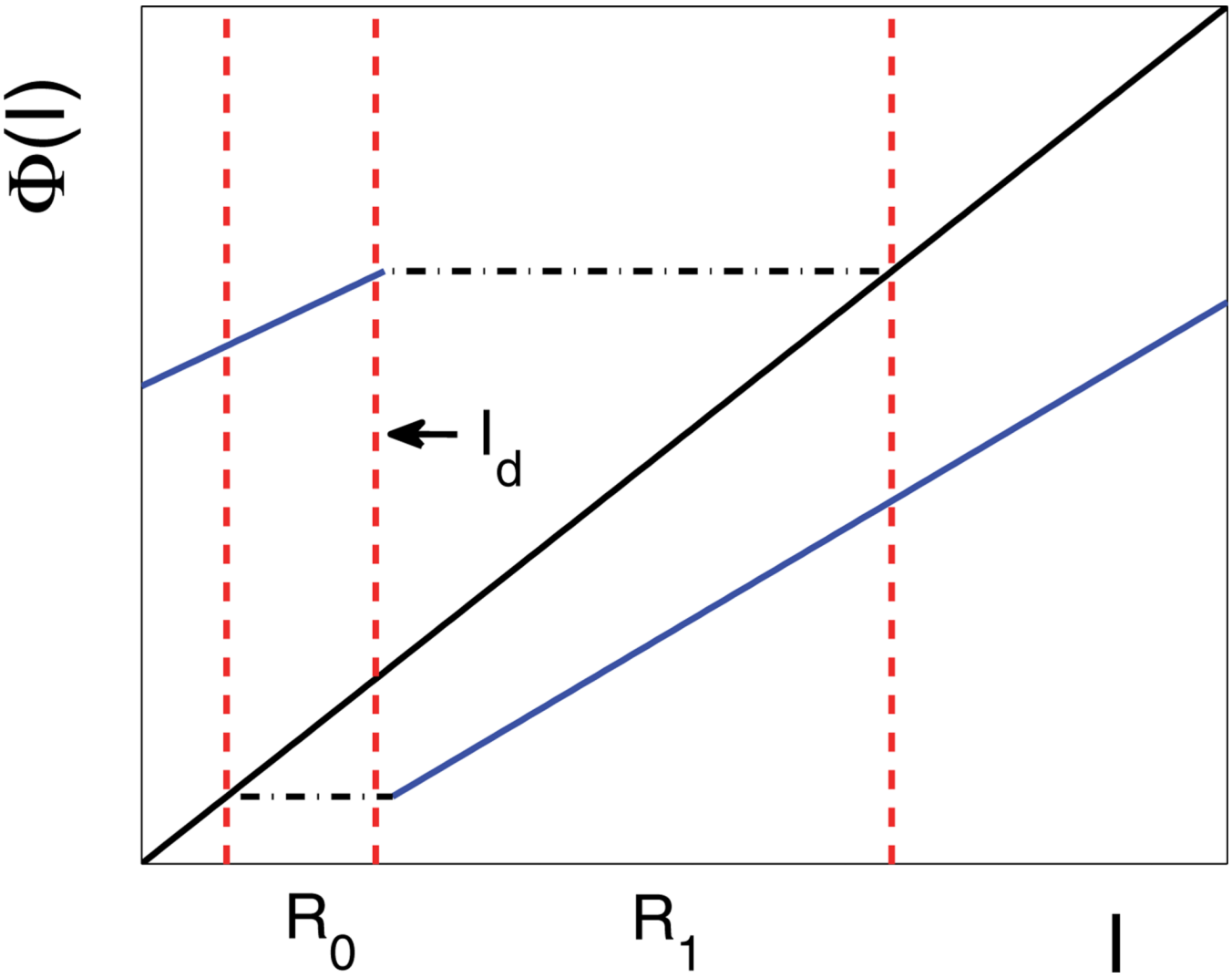

Figure 5.
The construction of the reachable sets is illustrated. As discussed, we may limit our analysis to the reachable set $R = R_0 \cup R_1$. Note that Φ is injective on R but not injective on the entire domain.

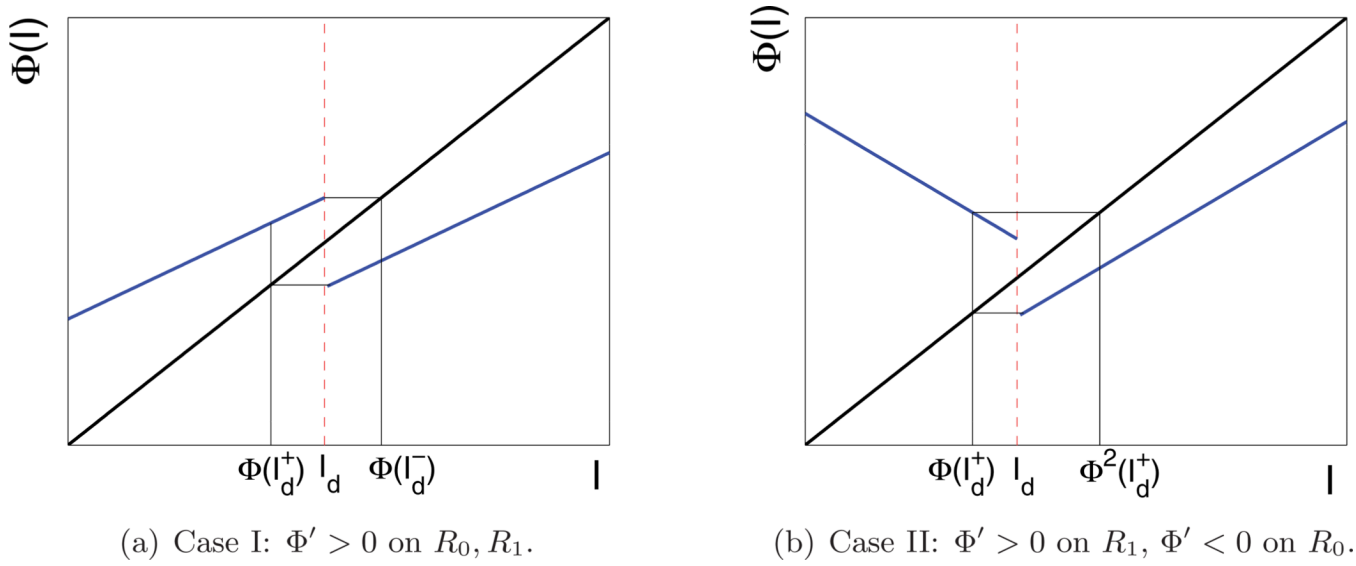

(a) Case I: $\Phi' > 0$ on R_0, R_1. (b) Case II: $\Phi' > 0$ on R_1, $\Phi' < 0$ on R_0.

Figure 6.

Illustration of Lemma 5.8 for a bursting map in which $\Phi : \mathrm{R} \to \mathrm{R}$ is not injective. We see that if Φ is piecewise injective on R, we can restrict the domain of Φ to a refined reachable set R' for which $\Phi : \mathrm{R}' \to \mathrm{R}'$ is injective.

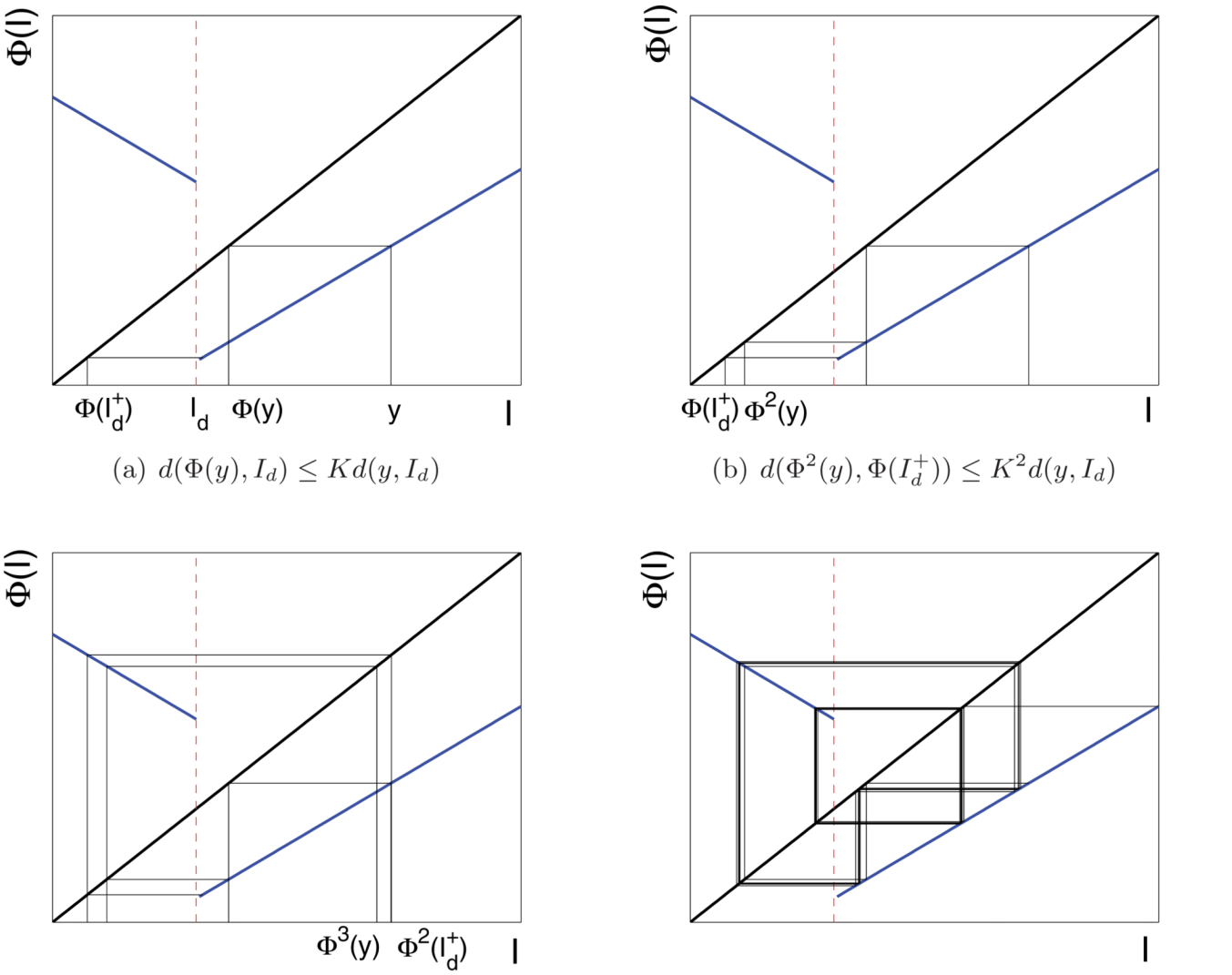

(a) $d(\Phi(y), I_d) \leq K d(y, I_d)$

(b) $d(\Phi^2(y), \Phi(I_d^+)) \leq K^2 d(y, I_d)$

(c) $d(\Phi^3(y), \Phi^2(I_d^+)) \leq K^3 d(y, I_d)$

(d) This plot shows the co-existence of two bursting frequencies in a single map.

Figure 7.

Illustration of Theorem 5.9 for a piecewise contractive map with Lipschitz constant 1 > K ≥ 0. In this case, the orbit of y is approached arbitrarily closely by the orbit of $\Phi(I_d^+)$.

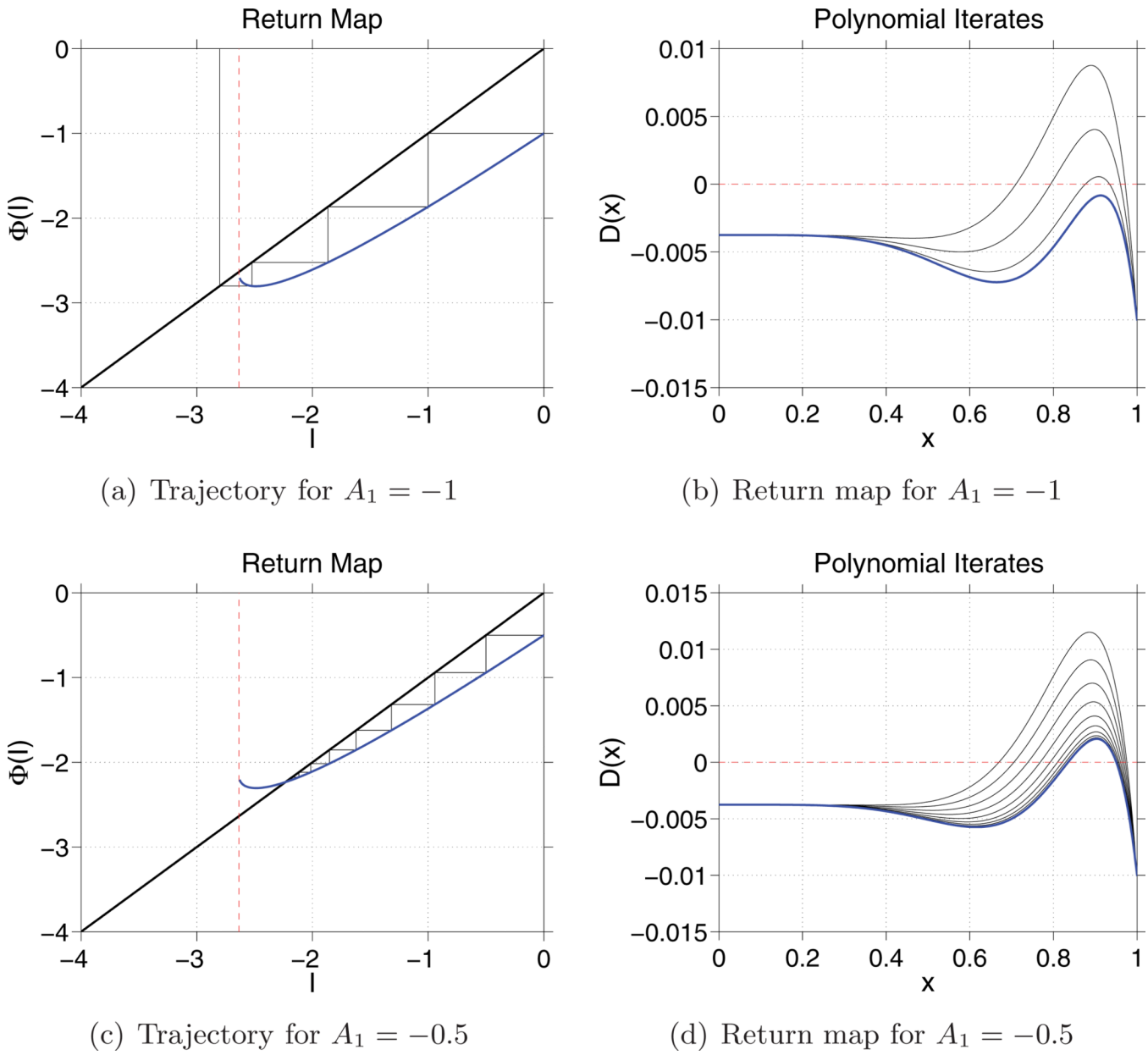

(a) Trajectory for $A_1 = -1$ (b) Return map for $A_1 = -1$

(c) Trajectory for $A_1 = -0.5$ (d) Return map for $A_1 = -0.5$

Figure 8.

The onset of tonic spiking from phasic spiking. (a), (b) Phasic spiking regime. The return map here is defined only on a finite interval of I_1 from which threshold can be reached, given V (0) = V_0 and $I_2(0) = A_2$. (a) An example of a return map and iterates corresponding to a phasic spiking solution. (b) D(x) for the iterates of I_1 shown in (a). (c), (d) Co-existence of quiescence and tonic spiking. (c) An example of a return map and iterates converging to a tonic spiking solution. (d) D(x) for the iterates of I_1 shown in (c). Parameters for all plots were identical (see Table 1) except for the reset parameter A_1. In (a), (c), the return map is defined only for I_1 above the value at the dashed vertical line. That is, threshold is never reached for $I_1(0)$ below this vertical line. In (b), (d), the blue line shows the iterate of D(x) computed at the final iterate shown in (a), (b), respectively.

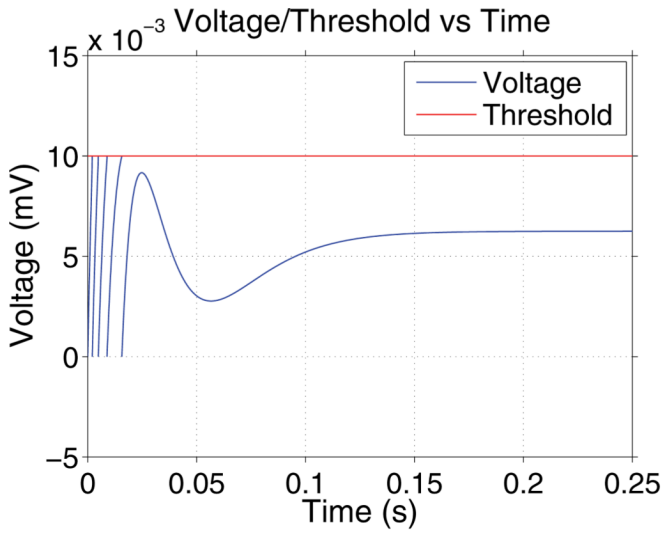

(a) Trajectory for $I_e = 0.35$

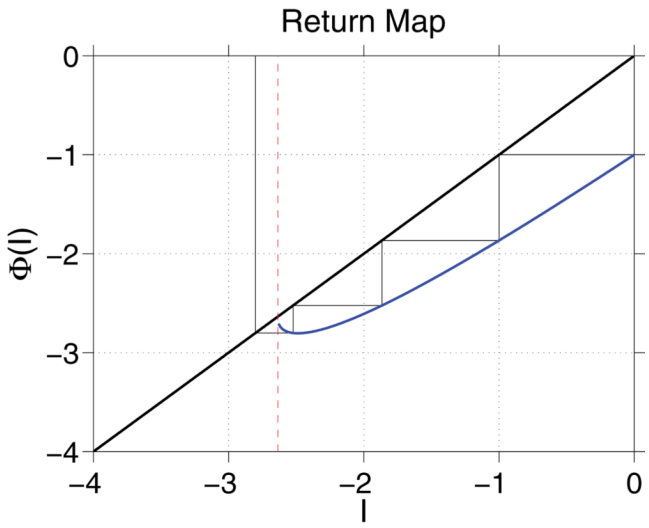

(b) Return map for $I_e = 0.35$

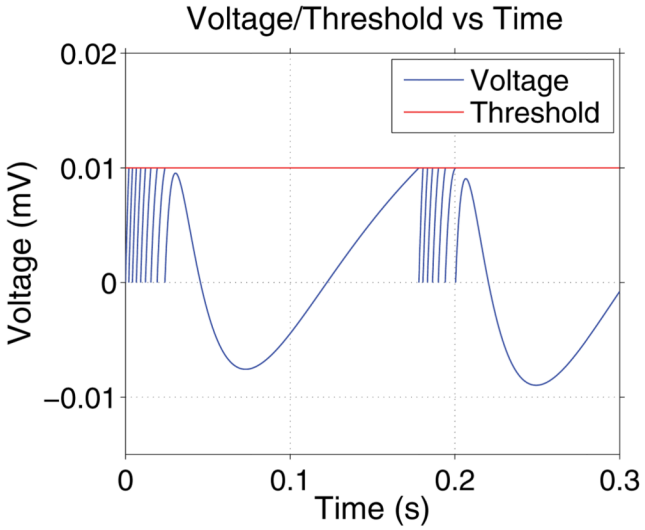

(c) Trajectory for $I_e = 1.0$

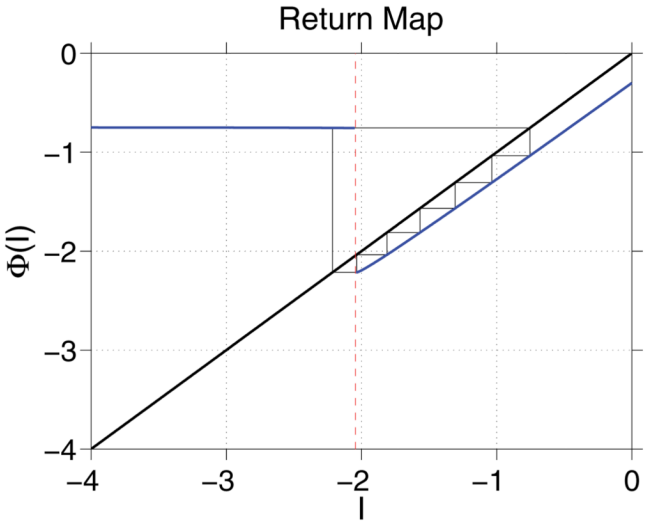

(d) Return map for $I_e = 1.0$

Figure 9.
Example of a bifurcation from phasic spiking to bursting as I_e is varied. (a), (b) At $I_e = 0.35$, all initial conditions lead to quiescence or phasic spiking and the return map Φ is defined only on a finite interval of I_1 values. (c), (d) At $I_e = 1.0$, (2.7) holds, spikes occur for all initial conditions I_{10}, Φ still has a discontinuity, and a periodic bursting solution exists. See Table 1 for other parameter values used.

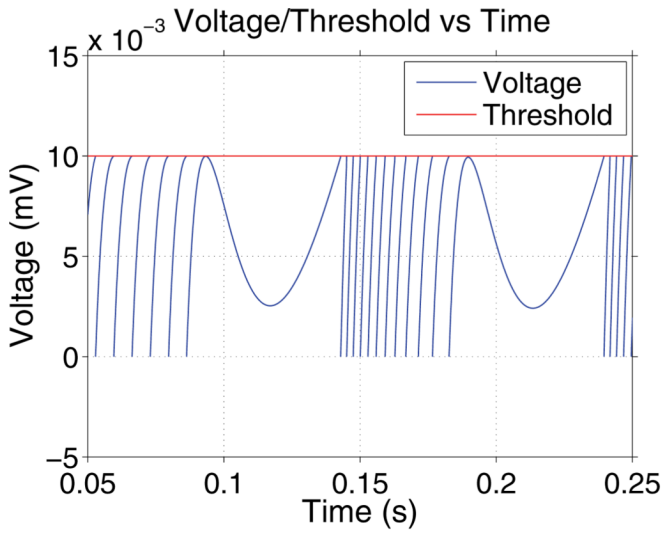

(a) Trajectory for $I_e = 3.5$

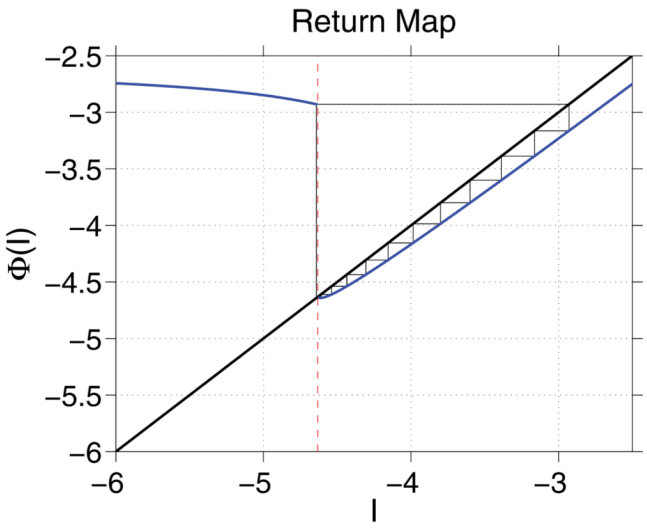

(b) Return map for $I_e = 3.5$

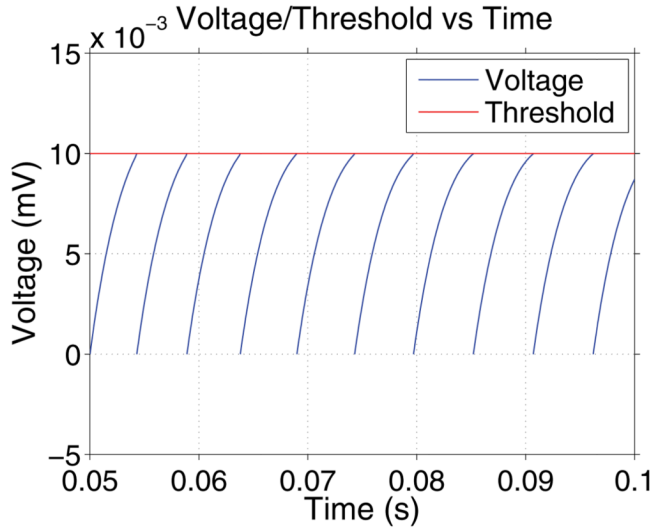

(c) Trajectory for $I_e = 4.5$

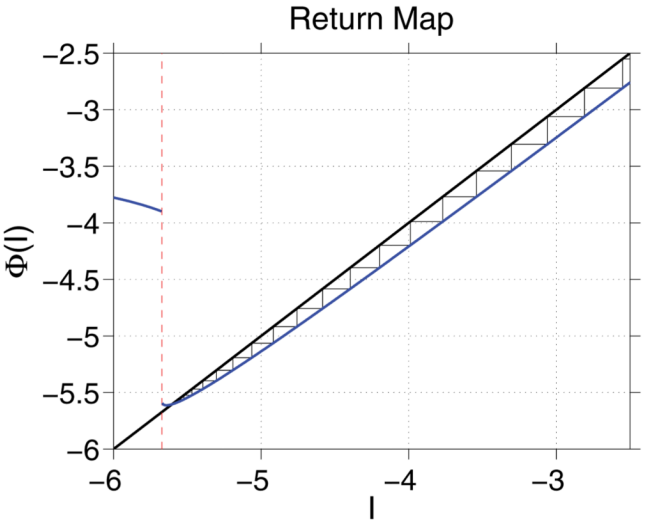

(d) Return map for $I_e = 4.5$

Figure 10.
Example of a border collision bifurcation caused by increasing the I_e. (a), (b) Bursting regime with $I_e = 3.5$. (c), (d) Tonic spiking regime with $I_e = 4.5$. See Table 1 for other parameter values used.

Table 1

Figures and parameter values used to generate them.

Figure(s)	I_e	A_1	A_2	k_1	k_2	γ	V_0	Θ
1(a), 3(a)–3(c)	3	−1.2	6	40	60	20	0	0.02
1(b)	3	−1.6	1	50	20	30	0	0.01
1(c)	6	−3.6	2	5	50	1	0	0.02
1(d), 4(a)–4(c)	3	−0.8	5	10	200	40	0	0.01
1(e)	3	−1.2	5	10	200	40	0	0.01
1(f)	3	−1.2	1	5	50	1	0	0.01
9(a)–9(d), 10(a)–10(d)	-	−0.3	5	10	200	40	0	0.01
8(a)–8(d)	0.5	-	5	50	100	80	0	0.01

Table 2

Parameter ranges for the numerical search of the piecewise contractive property of model neurons. Parameter sets are written using MATLAB syntax: [0 : 1 : 5] = [0, 1, 2, 3, 4, 5], for instance.

I_e	1:10
γ	20:20:60
k_1	40:20:200
k_2	40:20:200
Θ	0.020:0.005:0.025
I_1	−10:0.001:0
I_2	0:2:4